Theoretical analysis on detonation initiation induced by thermal nonuniformity in a supersonic flow

Dehai Yu [1,2,3] Pengfei Yang [1,2,3] Lianjie Yue,[1,2] and Zheng Chen [3,*]

[1]*State Key Laboratory of High Temperature Gas Dynamics, Institute of Mechanics,*
Chinese Academy of Sciences, Beijing 100190, China
[2]*School of Engineering Sciences, University of Chinese Academy of Sciences, Beijing 100049, China*
[3]*HEDPS, SKLTCS, College of Engineering, Peking University, Beijing 100871, China*

Detonation initiation in a supersonic reactive flow constitutes a crucial problem in fundamental combustion research and meanwhile receives great attention in the application of detonation-based propulsion systems. In this paper, we conduct theoretical analysis on detonation initiation induced by thermal nonuniformity. The underlying mechanism for detonation initiation is attributed to the self-strengthening coupling between the reaction front and the induced shock wave. A detonation initiation factor is introduced to quantify the capability of the thermal nonuniformity in causing detonation initiation. The initiation factor changes nonmonotonically, with the temperature difference describing the thermal nonuniformity. We find that there exist three regimes of detonation initiation. A threshold temperature difference of the thermal nonuniformity below which detonation initiation cannot take place is identified. Additionally, it is found that the temperature profile of the thermal nonuniformity has a substantial impact on detonation initiation. The creation of an additional induced shock wave on the reaction front due to the downward convex temperature profile significantly improves the initiation condition for weak thermal nonuniformities with relatively small temperature difference. Moreover, two-dimensional analysis is also conducted, considering the convective transport in the transverse direction. It is shown that the transverse heat transfer reduces the curvature of the reaction front, which promotes (inhibits) detonation initiation for strong (weak) thermal nonuniformity with large (small) temperature difference. In the present analysis, we provide useful insights into detonation initiation in a supersonic reactive flow.

I. INTRODUCTION

Combustion waves in flammable mixtures can be categorized into two modes: deflagration and detonation. According to gas dynamics of reactive flow, propagation of deflagration in a combustible mixture leads to little change in pressure, while the passage of detonation causes considerable increase in pressure due to the shock compression [1–3]. The inner structure of deflagration/premixed flame is dominated by chemical reaction and molecular transport (i.e., heat conduction and mass diffusion), whose balance determines the subsonic flame propagation speed relative to unburned gas [2,4]. Unlike deflagration, detonation propagates in supersonic speed, and molecular transport has little influence on detonation propagation. The inner structure of detonation relies on the self-strengthening interaction between the leading shock wave and the subsequent reaction zone [4,5].

---

*Contact author: cz@pku.edu.cn

Compared with deflagration, detonation helps to achieve faster heat release rate, higher thermal efficiency, and more compact engine structure [6,7]. Therefore, detonation has promising applications in propulsion systems. There are mainly three types of detonation engines, i.e., pulsed detonation engines (PDEs) [8,9], rotating detonation engines (RDEs) [10,11] and oblique detonation engines (ODEs) [12,13]. A PDE consists of a long tube filled with reactive mixture, which is ignited by a strong energy source. The resulting deflagration accelerates and eventually transitions to detonation, producing high pressure that is converted into thrust. Subsequent to completion of the reactant, the tube should be resupplied with fresh mixture and ignited again, and the engine enters a new cycle [6]. In the cylindrical combustion chamber of an RDE, a detonation wave propagates in the azimuthal direction, converting the reactant mixture into hot products and releasing heat [10]. In contrast with periodic refueling and detonation initiation in a PDE, the fuel and oxidizer are constantly injected into the combustion chamber, allowing the detonation to propagate continuously. As a result, an RDE can provide continuous thrust [14]. Despite analogous configuration between an ODE and a scramjet, i.e., the hypersonic inflow is compressed by an oblique shock wave at the inlet of the engine, the subsequent combustion process differs essentially. In the case of an ODE, the combustible mixture is converted into a hot product via an oblique detonation wave instead of combustion stabilized by flame holders such as a strut and a cavity in a scramjet [15]. Because of the self-strengthening behavior between the leading shock wave and the following reaction zone, the combustion process through oblique detonation tends to be more vigorous and robust [16]. Moreover, compared with PDEs and RDEs, an ODE is more suitable for hypersonic flight with a higher Mach number [16].

Detonation initiation plays an important role in the performance of detonation engines. There exist two basic approaches for detonation initiation, i.e., direct initiation [17,18] and deflagration-to-detonation transition (DDT) [19,20]. Direct initiation requires a significant amount of external energy input at a sufficiently high power [21]. Clarke *et al.* [22] conducted a theoretical study on the direct initiation of planar detonation. They thoroughly analyzed the characteristic time scales of the principal processes, such as the acoustic wave propagation, unsteady heat conduction from the igniting source, and chemical reaction. He and Clavin [18] developed a criterion for the direct initiation of cylindrical and spherical detonations by a localized ignition source. A critical initiation radius was identified, above which detonation can propagate outwardly in a self-sustained manner.

The energy of direct detonation initiation is exceedingly higher than that for conventional ignition of deflagration [19,21]. The difficulty of direct initiation implies that detonation usually results from the DDT process in practical situations. Ciccarelli and Dorofeev [23] gave a review on DDT and demonstrated that DDT consists of two stages, i.e., the creation of a suitable condition for detonation onset and the subsequent detonation development. The second stage of detonation development is mainly induced by the reactivity gradient of the combustible mixture. According to the gradient theory of Zel'dovich [24], the propagation speed of reaction front u_{front} is inversely proportional to the gradient of ignition delay time τ_{ig}, i.e., $u_{front} \sim (\nabla \tau_{ig})^{-1}$. Five modes of reaction front propagation were identified, i.e., thermal explosion or homogeneous autoignition, supersonic reaction front propagation, detonation development, subsonic reaction front propagation, and deflagration. Detonation initiation requires the strong coupling between the chemical reaction and its induced shock wave, which in general results from continuous collapse of compression waves propagating at the speed of sound $u_{acoustic}$ [25]. Therefore, the critical condition for detonation initiation can be interpreted as $u_{acoustic} \sim u_{front}$, at which the coherent coupling between the chemical reaction and the pressure wave occurs [24,26]. Lee *et al.* [21] proposed a generalized interpretation to the spontaneous transition from deflagration to detonation without an external ignition source based on the so-called shock wave amplification by coherent energy release mechanism. The preparation of a suitable condition for detonation wave onset can be achieved through multiple routes [27–29] since the reaction rate and ignition delay time depend on temperature and pressure as well as the mixture composition [30,31]. Authors of existing studies have demonstrated that detonation development can be induced by thermal stratification in a hot or cool spot [27,32] and by spatially varying the equivalence ratio [33,34].

The reaction rate constant usually exhibits in Arrhenius form with large activation energy being sensitive to temperature variation. Therefore, thermal nonuniformity or thermal stratification has a great impact on reaction front propagation and plays a decisive role in detonation initiation. Gu *et al.* [26] studied the autoignition of stoichiometric H_2/CO/air mixtures. They proposed the detonation peninsula for detonation development induced by a hot spot in terms of a normalized temperature gradient in the hot spot ξ. Dai *et al.* [35,36] analyzed the autoignition and detonation formation in hydrocarbon/air mixtures by a hot spot through a series of numerical studies. In addition, numerical simulations showed that detonation development induced by autoignition in a hot spot may produce strong pressure oscillation in a closed chamber, which is known as super knock. Such a phenomenon can be alleviated by arranging the temperature gradient of the hot spot so that detonation development is induced by shock/pressure waves reflected from the end wall. Pan *et al.* [37] conducted numerical simulations to identify a detonation peninsula for different fuels. Luong and Im [38] conducted two-dimensional simulations on the detonation development regime induced by temperature inhomogeneities under engine conditions. They proposed a revised model which considers the multidimensional effect resulting from the interaction and collision of multiple ignition kernels. In addition, the effects of a negative temperature coefficient were assessed by adopting dimethyl ether as a fuel.

The above studies on detonation initiation induced by a hot spot are mainly related to super knock occurring in internal combustion engines. In those studies, the reactant was assumed to be quiescent or to have low flow speed. However, in typical detonation engines, such as an ODE, the combustion process is always associated with supersonic airstream, which leads to a series of intensive compressive waves [39–41]. The ensuing shock-shock and shock-reaction front interactions inevitably lead to spatially dispersed thermal nonuniformities. Therefore, it is important to understand detonation initiation due to thermal nonuniformity in a supersonic reactive flow. Such a topic receives little attention in the literature and is address in this paper.

Unlike in previous studies in quiescent environments [26,35,36], in this paper, we emphasize the interaction between shock waves and reaction fronts in supersonic reactive. The objective of this paper is to interpret the process of detonation development induced by thermal nonuniformity, advancing fundamental understandings of the mechanism underlying detonation initiation. The flow velocity contributes to the continuous formation and collapse of compression waves, thereby intensifying or weakening the shock-reaction front coupling depending on the temperature difference characterizing the thermal nonuniformity. Specifically, we present a theoretical and numerical study on the interaction between the reaction front and the induced shock wave resulting from spatially varying the temperature profile. The capability of the thermal nonuniformity leading to detonation initiation is examined by analyzing the intensity of the interaction between the reaction front and the induced shock wave. This paper is organized as follows. In Sec. II, the theoretical model describing the detonation initiation is introduced. In Sec. III, the process of detonation initiation is analyzed based on the simplified one-dimensional model, neglecting the convective transport in the transverse direction. The initiation factor $\eta_{\mathrm{initiation}}$ is proposed to quantify the capability of the thermal nonuniformity, leading to the appearance of detonation wave in supersonic reactive flow. In Sec. IV, a two-dimensional formulation is proposed, considering the convective transport in the transverse direction. The effects of transverse convection on detonation initiation are assessed. Concluding remarks are given in Sec. V.

II. THEORETICAL MODEL

The governing equations for the reactive supersonic flow are based on the conservation laws of mass, momentum, energy, and species. Specifically, they are given as the following:

Continuity equation:

$$\frac{\partial \rho}{\partial t} + \nabla \cdot (\rho \mathbf{u}) = 0, \tag{1}$$

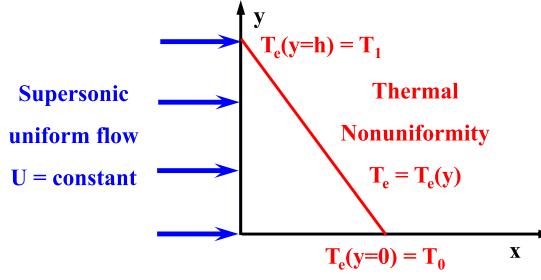where ρ is the density, and $\mathbf{u}$ the velocity vector;

FIG. 1. Schematic of the thermal nonuniformity in supersonic uniform flow.

Momentum equation:

$$\rho \frac{\partial \mathbf{u}}{\partial t} + \rho \mathbf{u} \cdot \nabla \mathbf{u} = -\nabla p + \nabla \cdot \boldsymbol{\tau}, \tag{2}$$

where p is the pressure, $\boldsymbol{\tau}$ the viscous stress tensor;

Energy equation:

$$\rho c_p \left(\frac{\partial T}{\partial t} + \vec{u} \cdot \nabla T \right) = \nabla \cdot (\lambda \nabla T) + \Phi + \dot{q}, \tag{3}$$

where c_p is the heat capacity at constant pressure, λ the thermal conductivity, T the temperature, Φ the viscous dissipation rate, and $\dot{q}$ the heat release rate from chemical reactions;

Species equation:

$$\rho \frac{\partial Y_i}{\partial t} + \rho \mathbf{u} \cdot \nabla Y_i = \nabla \cdot (D_i \nabla Y_i) + \dot{\omega}_i, \tag{4}$$

where Y_i is the mass fraction of species i, D_i the diffusion coefficient of species i, and $\dot{\omega}_i$ the rate of production (or consumption) of species i due to chemical reaction.

In this paper, we aim to assess the fundamental mechanism of oblique detonation initiation by thermal nonuniformity imbedded in a supersonic and uniform reactive flow at velocity U. The schematic is shown in Fig. 1. The thermal nonuniformity is represented by a specific temperature profile in the traverse direction (i.e., the y direction). For analytical tractability, we have made a few assumptions and simplifications:

(1) Streamwise dominance: The streamwise direction of the uniform supersonic flow is assumed to coincide with the x direction. This assumption enables the reduction of the governing equations to a one-dimensional form along the x direction, primarily considering the convective effects in the streamwise direction while neglecting the transverse velocity components. This simplification is valid for high Mach number flows where the streamwise momentum dominates, and the transverse velocity components are relatively small.

(2) Negligible viscous and conductive effects: In supersonic flows, particularly those involving high Mach numbers, the effects of viscous stresses and heat conduction are small compared with the convective transport of mass, momentum, and energy. The characteristic time scales for heat conduction $t_{\text{conduction}} \sim L^2/\alpha$ and mass diffusion $t_{\text{diffusion}} \sim L^2/D$, where α is the thermal diffusivity and D is the mass diffusivity of the mixture, are significantly larger than the acoustic time scale $t_{\text{acoustic}} \sim L/a_e$, where L is a characteristic length and a_e is the speed of sound at the inlet. The ratio $t_{\text{acoustic}}/t_{\text{conduction}}$ (or $t_{\text{acoustic}}/t_{\text{diffusion}}$) is proportional to the Knudsen number Kn [42], which is very small (i.e., Kn $\ll 1$) in the continuum limit. Therefore, viscous and conductive effects are neglected, allowing the formulation to be based on the Euler equations.

(3) Constant properties: The thermophysical properties such as specific heat capacity c_p, thermal conductivity λ, and diffusivity coefficients α and D are assumed to be constant throughout the flow. This assumption simplifies the analysis by focusing on the essential effects of chemical reactions
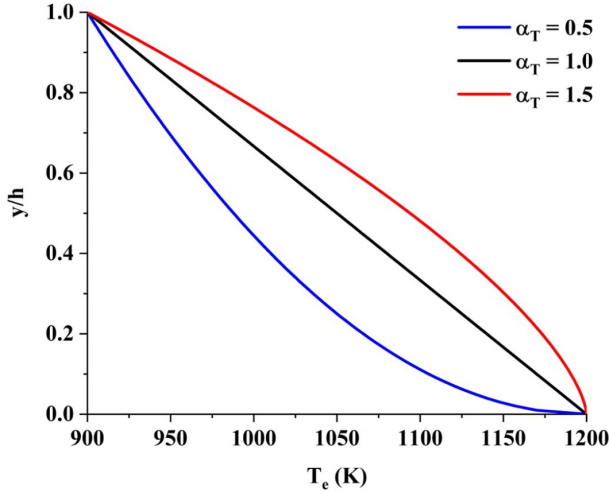
FIG. 2. Various temperature distributions at the inlet of the supersonic flow characterized by the geometric parameters α_T. The temperatures at two boundaries are $T_e(y = 0) = T_0 = 1200$ K and $T_e(y = h) = T_1 = 900$ K.

and flow dynamics without introducing additional complexities associated with variable properties, which may change significantly with temperature or pressure variations.

(4) Steady-state assumption: The flow is assumed to reach a steady state, wherein all flow properties, e.g., velocity, pressure, temperature, and species concentration, are functions of spatial coordinates. By assuming steady-state conditions, the time derivatives in the conservation equations are set to zero, reducing the complexity of the mathematical formulation and focusing on the balance between convective transport, chemical reactions, and other relevant processes in the flow field.

For mathematical simplicity, we adopt the one-step model to describe the chemical reaction:

$$F \rightarrow P + Q, \tag{5}$$

where F refers to reactant, P the product, and Q the chemical heat per unit mole of reactant. The reaction rate follows the Arrhenius law:

$$\omega = Bc_F \exp\left(-\frac{T_a}{T}\right), \tag{6}$$

where B is the frequency factor and T_a the activation temperature, and T and c_F, respectively, are the temperature and molar concentration of the reactant.

The thermal nonuniformity is characterized by the temperature distribution at the entrance, which can be modeled in the following form, i.e.,

$$T_e = T_0 - (T_0 - T_1)\left(\frac{y}{h}\right)^{\alpha_T}, \tag{7}$$

where T_0 and T_1 refer to the temperatures at the lower and upper bounds, respectively, h the spatial dimension of the thermal nonuniformity, and α_T a geometric parameter that determines the geometry of the temperature distribution. Depending on thermodynamic and fluid dynamic conditions, the temperature profile could be either upward convex (corresponding to $\alpha_T > 0$) or downward convex (corresponding to $\alpha_T < 0$), as indicted in Fig. 2. Particularly, the linear temperature profile is reproduced by setting $\alpha_T = 1.0$. In this paper, we consider the case of $T_0 > T_1$ and fixed $T_0 = 1200$ K.

Before conducting theoretical analysis, the boundary conditions of the supersonic flow should be specified, and the key assumptions and simplifications must be addressed. In this theoretical model,

we assumed isobaric conditions, i.e., $p = p_e$, at the entrance $x = 0$ upstream of the reaction front, where the mixture remains in a nearly frozen state, without significant heat release or transverse heat conduction. This simplification allows us to define a uniform pressure distribution across the transverse direction at the entrance, compatible with the isobaric parallel flow assumption. However, nonzero transverse temperature gradient $T = T_e(y)$ implies a corresponding transverse density gradient, i.e., $\rho_e(y) = p_e/[(\gamma - 1)T_e(y)]$. This transverse density gradient complicates the flow dynamics, especially when the chemical heat release ($\omega \neq 0$) disrupts the initial isobaric condition. The inclusion of this transverse density gradient in the flow field formulation is crucial to accurately capturing the effects of thermal nonuniformity and transverse heat transfer on the detonation initiation mechanism. However, due to mathematical complexities, a comprehensive interpretation of the influence of density gradient during detonation initiation process is beyond the scope of the current theoretical model.

The boundary conditions at the entrance [$x = 0$: $T = T_e(y)$, $p = p_e$, $u = U$, and $v = 0$] represent an idealized case, which is intended to simplify the theoretical framework and enable analytical tractability. In practice, achieving such conditions for a high-temperature reactive mixture with a short induction time is challenging due to the difficulty in maintaining a uniform transverse temperature gradient and pressure distribution in real-world scenarios. However, we also noted that temperature nonuniformity in supersonic flows is a common phenomenon in hypersonic air-breathing engines, where air entering the combustor at supersonic speeds undergoes uneven heating due to compression, shock-boundary layer interactions, and localized heat release [43,44]. These processes naturally lead to nonuniform temperature fields, which can significantly affect ignition and flame stability, creating complex combustion dynamics similar to the thermal nonuniformities modeled in this paper. Adopting such idealized boundary conditions, the current theoretical model isolates the key mechanisms driving the initiation process without the added complexities of variable boundary conditions. This approach allows us to derive fundamental insights into the physics of detonation initiation that might be obscured by the numerous interacting factors present in real-world scenarios. These idealized conditions serve as a necessary baseline for theoretical analysis, providing a controlled environment to understand the primary effects of thermal nonuniformity on detonation initiation.

In reactive flow, a chemical reaction proceeds in association with the motion of a fluid element in the streamwise direction. According to Rayleigh's criterion [45], the heat release from an exothermic reaction produces pressure waves, which leads to fluid element movement in the transverse direction. Thus, the passage of supersonic reactive flow through thermal nonuniformity is a two-dimensional problem. Nevertheless, the uniform flow at the inlet is highly supersonic, which allows us to assume streamwise dominance of the flow field, i.e., the transverse velocity is substantially smaller than that in the streamwise direction. Based on this hypothesis, the governing equations can be simplified into one-dimensional form by neglecting the convective heat and mass transfer in the transverse direction. The simplified one-dimensional problem is considered in the next section. The rigorous two-dimensional analysis considering transverse convection shall be discussed in Sec. IV.

III. ONE-DIMENSIONAL ANALYSIS ON DETONATION INITIATION

A. Reaction front profile

Supersonic reactive flow passing through the thermal nonuniformity at the entrance results in autoignition at certain streamwise distance, which depends on the transverse elevation y. This indicates that the coordinates corresponding to autoignition onset constitute a two-dimensional curve, which anchors in the flow field when steady state is achieved after a sufficiently long time. Adopting the simplifications (1)–(4), the governing equations are reduced to steady, two-dimensional Euler equations. In this section, we may first neglect the interaction between adjacent streamlines and regard the transverse coordinate as a parameter, while this parameter varies with

initial temperature T_e of the fluid element entering the supersonic flow field. Converting the mass fraction to concentration in the species equation, the mathematical formulation can be organized in one-dimensional form, i.e.,

$$\rho c_p U \frac{dT}{dx} = Q\omega, \tag{8}$$

$$U \frac{dc_F}{dx} = -\omega. \tag{9}$$

In terms of the spatial dimension of the thermal nonuniformity h and the uniform flow velocity U, we define the nondimensional coordinates and time as

$$\tilde{x} = \frac{x}{h}, \quad \tilde{y} = \frac{y}{h}, \quad \tilde{t} = \frac{tU}{h}. \tag{10}$$

In reactive flow, the temperature variation within a fluid element is primarily due to chemical heat release. Therefore, the nondimensional temperature and normalized reactant molar concentration are conventionally defined as

$$\tilde{T} = \frac{T}{\Delta T_{\text{reaction}}}, \quad \tilde{c}_F = \frac{c_F}{c_{F0}}, \tag{11}$$

where c_{F0} is the molar concentration of the reactant at the entrance (i.e., $\tilde{x} = 0$), and $\Delta T_{\text{reaction}}$ is the increase of temperature due to chemical reaction, i.e., $\Delta T_{\text{reaction}} = Qc_{F0}/\rho c_p$. A conserved coupling function can be constituted as $\beta = \tilde{T} + \tilde{c}_F$ satisfying

$$\frac{d\beta}{d\tilde{x}} = 0. \tag{12}$$

Solving Eq. (12) subject to boundary conditions $\tilde{T}(\tilde{x} = 0, \tilde{y}) = \tilde{T}_e(\tilde{y})$ and $\tilde{c}_F(\tilde{x} = 0, \tilde{y}) = 1$, we have the following linear correlation between $\tilde{T}$ and $\tilde{c}_F$:

$$\tilde{c}_F = 1 + \tilde{T}_e - \tilde{T}. \tag{13}$$

Substituting Eq. (13) into Eq. (8) and organizing in nondimensional form, we obtain

$$\frac{d\tilde{T}}{d\tilde{x}} = \tilde{B}(1 + \tilde{T}_e - \tilde{T}) \exp\left(-\frac{\tilde{T}_a}{\tilde{T}}\right), \tag{14}$$

where $\tilde{B} = Bh/U$ is the nondimensional reaction frequency factor. For reactive flow, the chemical reaction proceeds as the fluid element moves downstream. The reaction length $\tilde{L}_{\text{reaction}}$ is defined as the nondimensional distance from the inlet to the streamwise coordinate where the reactant is completely depleted. Due to large activation temperature, a vigorous reaction is concentrated at an extremely thin region in the vicinity of $\tilde{x} = \tilde{L}_{\text{reaction}}$. Because of thermal nonuniformity, the reactivity of fluid elements varies across different streamlines. It suggests that the reaction length $\tilde{L}_{\text{reaction}}$ shall be treated as a function of the transverse coordinate, i.e., $\tilde{L}_{\text{reaction}} = \tilde{L}_{\text{reaction}}(\tilde{y})$. The analytical expression of the reaction length can be obtained by integrating Eq. (14), yielding

$$\tilde{L}_{\text{reaction}}(\tilde{y}) = \frac{1}{\tilde{B}} \int_{\tilde{T}_e}^{1+\tilde{T}_e} \frac{\exp(\tilde{T}_a/\tilde{T})}{1 + \tilde{T}_e - \tilde{T}} d\tilde{T}. \tag{15}$$

The integral on the right-hand side diverges as $\tilde{T} \to 1 + \tilde{T}_e$, which can be attributed to the substantial fall of the reaction rate due to depletion of the reactant in the mixture. It leads to a long streamwise distance over which the reactant concentration remains infinitesimally low and thus should not be included in the reaction length. Therefore, the upper limit of the integral in Eq. (15) should be revised to $1 + \tilde{T}_e - \epsilon$, with $\epsilon \ll 1$, to cut off the unphysical long tail of reaction length. In this paper, the parameter ϵ is fixed to be $\epsilon = 0.001$, and it has been tested that the reaction front remains unaltered with further reducing of the magnitude of ϵ. Obtaining a finite reaction length by adjusting the upper limit of the integral on the right-hand side of Eq. (11) is an artificial
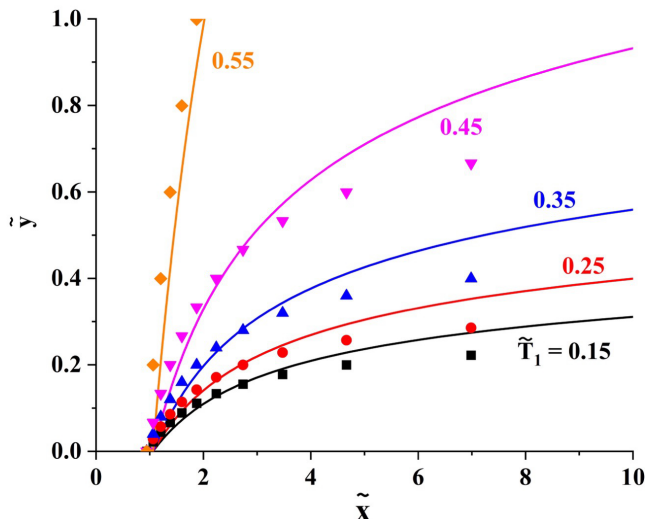
FIG. 3. The reaction front in a supersonic flow of a stoichiometric hydrogen/air mixture subject to linear temperature profiles with $\tilde{T}_0 = 0.6$. The scattered symbols refer to numerical simulation results corresponding to individual upper boundary temperatures, i.e., black squares for $\tilde{T}_1 = 0.15$, red circles for $\tilde{T}_1 = 0.25$, blue upward triangles for $\tilde{T}_1 = 0.35$, purple downward triangles for $\tilde{T}_1 = 0.45$, and orange diamonds for $\tilde{T}_1 = 0.55$. The lines represent results predicted by Eq. (11).

approach and does not correspond to the induction length in a rigorous sense. It is noted that, in the context of a one-step Arrhenius law with a large reduced activation energy ($\beta = T_a/T_0 \gg 1$), the induction length should be defined in the limit $\beta \to \infty$ using a small relative increase in temperature $(T - T_e)/T_e = 1/\beta$, as established in detonation theory. This definition provides a precise characterization of the induction length, distinguishing it from the total reaction length, which comprises both the induction and heat release zones, such that $L_{\text{reaction}} = L_{\text{induction}} + L_{\text{heat-release}}$. Due to the large activation energy, the heat release zone is highly localized and significantly shorter than the induction length, i.e., $L_{\text{heat-release}} \ll L_{\text{induction}}$. In the asymptotic sense, it is expected that $L_{\text{iduction}}/L_{\text{reaction}} \approx 1 - 1/\beta$. Thus, the current approach provides a reasonable approximation of the induction length, while the implications of employing the artificial cutoff method have been clarified to enhance the understanding of this approximation within the theoretical framework. We recognize that this method does not fully adhere to a rigorous large activation energy asymptotic analysis, which is indicated by the singularity when evaluating the reaction length using the integral in Eq. (11). This singularity arises due to the separation of induction length and heat-release length. The introduction of small parameter ϵ, avoiding numerical divergence in the integral calculation, allows a consistent approximation of the reaction front position. By adopting this approach, the model focuses on capturing the key interactions driving detonation initiation while balancing complexity and solvability.

In this paper, we consider a stoichiometric H_2/air mixture. For this mixture, the reaction rate frequency factor $B = 1.0 \times 10^8\,\text{s}^{-1}$ and activation temperature $T_a = 12\,800$ K are determined by fitting the ignition delay time calculated from simulation using detailed chemistry. Based on thermodynamic calculation, the temperature growth due to chemical reaction is around $\Delta T_{\text{reaction}} = 2000$ K.

The temperature profile at the entrance $T_e = T_e(y)$ is characterized by lower and upper temperatures $\tilde{T}_0$ and $\tilde{T}_1$ as well as the geometric parameter α_T. The reaction length at each transverse coordinate can be determined through Eq. (15). Figure 3 shows the reaction front curve corresponding to the linear temperature profile with $\alpha_T = 1.0$ and $\tilde{T}_e(\tilde{y} = 0) = \tilde{T}_0 = 0.6$ (i.e., $T_0 = 1200$ K). The reaction front constituted by the coordinates of ignition locations, i.e., $(\tilde{L}_{\text{reaction}}, \tilde{y})$ bends toward

the downstream direction when the upper boundary temperature falls. This is because the relatively lower temperature at a larger transverse coordinate results in significant reduction in the reaction rate and thus substantially elongates the reaction length.

To validate the theoretical predictions, we also conducted a numerical calculation of the reaction front induced by thermal nonuniformity, which is described by linear temperature distribution at the supersonic flow inlet. The detailed kinetic model developed by Burke *et al.* [46] for hydrogen is adopted, which incorporates 27 reversible elementary reactions involving nine species $(H_2, O_2, H_2O, H, O, OH, HO_2, H_2O_2,$ and $N_2)$. The thermodynamic properties of these species are evaluated using the nine-coefficient NASA polynomial formulas [47]. Though Fig. 3 shows quantitative difference between theoretical prediction (lines) and numerical results (symbols), which may be attributed to the simplified one-step chemical model adopted in the theoretical formulation, the variation trend of the reaction front predicted by theory agrees well with that from simulations.

B. Compressing Mach waves generation

The onset of autoignition in a combustible mixture is associated with substantial heat release from chemical reaction. It leads to sudden expansion of the fluid element and thereby produces compression waves [48]. In such a supersonic flow field, the compression waves can be treated as Mach waves which propagate at the Mach angle with the streamwise direction [49]. The Mach angle can be determined in terms of the Mach number M, i.e.,

$$\alpha_M = \arcsin \frac{1}{M}. \tag{16}$$

Because of thermal nonuniformity, the local sound speed changes along the transverse coordinate, and so does the Mach number and Mach angle. Consequently, the Mach waves originating from distinct points on the reaction front are not parallel with each other, and thereby, they may collapse, leading to shock wave formation on the downstream side of the reaction front.

For illustrative simplicity and clarity, we first consider the downstream behavior of two Mach waves originated from a pair of adjacent points R_1 and R_2 on the reaction front. To be specific, we consider that point R_2 locates beyond point R_1. Therefore, their coordinates $R_1 = (\tilde{x}_{r1}, \tilde{y}_{r1})$ and $R_2 = (\tilde{x}_{r2}, \tilde{y}_{r2})$ satisfy $\tilde{x}_{r1} < \tilde{x}_{r2}$ and $\tilde{y}_{r1} < \tilde{y}_{r2}$. The Mach wave can be considered a straight line whose slope k_s is determined by the Mach angle through $k_s = \tan(\alpha_M)$. Therefore, the coordinates of the Mach waves generated at points R_1 and R_2 can be written in the following form:

$$\tilde{y} - \tilde{y}_{ri} = k_{si}(\tilde{y} - \tilde{x}_{ri}), \quad i = 1, \ 2. \tag{17}$$

According to principles of compressible fluid flow, the slopes of the Mach waves depend upon the Mach number at the source point R_i, i.e.,

$$k_{si} = \frac{1}{\sqrt{M_i^2 - 1}}, \quad i = 1, \ 2. \tag{18}$$

Rigorously, the Mach number M_i should be calculated using the local temperature of the concerned point on the reaction front. However, it involves the complete solution of the temperature field in this reactive supersonic flow and thereby is exceedingly difficult to deal with analytically. For simplicity, we evaluate the Mach number based on the state at the entrance where the temperature distribution $\tilde{T}_e = \tilde{T}_e(\tilde{y})$ is given by Eq. (7). Accordingly, the slope of the Mach wave as a function of the transverse coordinate can be determined as

$$k_{si}(\tilde{y}) = \pm \frac{1}{\sqrt{M_e^2(\tilde{y}) - 1}}, \tag{19}$$

where $M_e(\tilde{y}) = U/\sqrt{\gamma R T_e(\tilde{y})}$ is the Mach number evaluated at the inlet of the supersonic flow field. Using the sound speed of the unburned gas to define the Mach angle for compression waves has certain limitations. The local sound speed varies significantly within the exothermal reaction
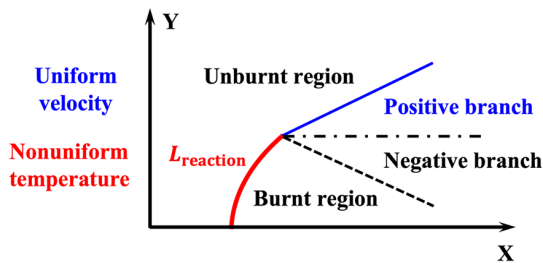
FIG. 4. Schematic of Mach wave generation from the reaction front.

zone due to substantial temperature changes. However, obtaining the local Mach number would require a complete solution of the temperature field in the reactive supersonic flow, which introduces considerable analytical complexity and is beyond the scope and analytical tractability of the current model. This simplified approach using the inlet state to define sound speed allows for a qualitative interpretation of the formation of compression waves and thus captures the essential behavior of the wave-reaction front interaction.

Regarding Eq. (19), there exist two branches of Mach waves extending transversely in upward and downward directions, which are characterized by the positive and negative signs on the right-hand side of Eq. (19), respectively. In this paper, only the positive branch shall be retained for consideration, which can be understood as follows. Because of the negative temperature gradient at the inlet [$T_0 > T_1$ in Eq. (3)], the fluid element entering the flow field at higher transverse elevation has a relatively lower reaction rate and thereby a longer reaction length, i.e., $\tilde{L}_{\text{reaction}}(\tilde{y}_2) > \tilde{L}_{\text{reaction}}(\tilde{y}_1)$ whenever $\tilde{y}_2 > \tilde{y}_1$. The reaction front is first initiated at $\tilde{y} = 0$ with the highest temperature and then advances in the transverse direction. Large activation energy of chemical reaction implies that the mixture is almost completely converted into a product at the downstream of $\tilde{L}_{\text{reaction}}$, releasing a significant amount heat. According to thermoacoustics, the chemical heat release leads to pressure wave generation, which in this paper is assumed to be compressing Mach waves, as shown in Fig. 4. The reaction front, denoted by the red solid line, and the streamline passing through the upper terminal of the reaction front, denoted by the dash-dot line, separate the reactive flow field into burnt and unburnt regions. The positive branch of the Mach line (the blue solid line) originates at the upper terminal of the reaction front and extends into the unburnt region, while the negative branch (black dashed line) shall be found in the burnt region.

This physical scenario provides an interpretation of the self-strengthening mechanism of detonation initiation [50,51]: The chemical reaction continuously generates compression waves that intensify the leading shock wave, and meanwhile, the shock wave accelerates the chemical reaction due to temperature and pressure elevation. The negative branch of the Mach wave develops into the burnt region without forming the positive feedback with subsequent chemical reaction. Therefore, we expect that the negative branch of the Mach wave may not play a decisive role in affecting the detonation initiation process. For a positive temperature gradient at the entrance, the scenario turns to be the opposite situation, and accordingly, the negative branch of the Mach wave should be considered.

C. Pressure waves and reaction front interaction

Given entrance temperature profile $\tilde{T}_e(\tilde{y})$, the slope of the Mach line originated from the points R_1 and R_2 can be calculated from Eq. (19). Rigorously, the Mach lines should be curves because the flow Mach number at the entrance varies due to thermal nonuniformity. Nevertheless, such a curvature is sequentially experienced by all compressing Mach waves generated on each segment of the reaction front as they propagate in the unburnt region. Therefore, we may assume that the
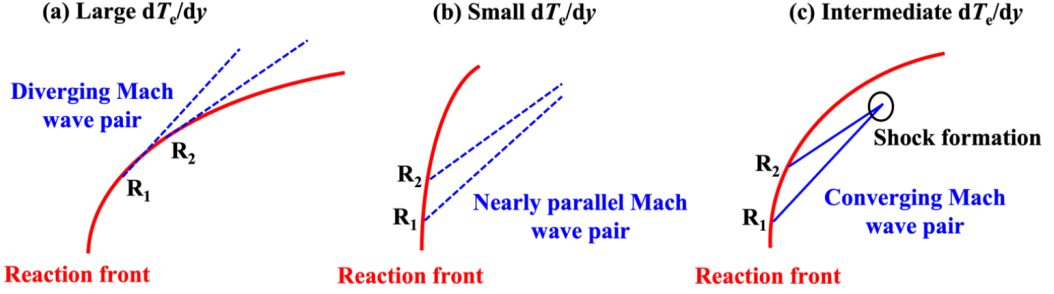
FIG. 5. Schematics for three situations of shock wave formation by Mach wave collapse: (a) large, (b) small, and (c) intermediate temperature gradients at the supersonic flow entrance.

compressing Mach waves are straight lines. These nonparallel Mach lines described by Eq. (17) come cross at some point, whose coordinate can be determined as

$$\tilde{x}_s = \frac{k_{s1}\tilde{x}_{r1} - k_{s2}\tilde{x}_{r2} - \tilde{y}_{r1} + \tilde{y}_{r2}}{k_{s1} - k_{s2}}, \tag{20}$$

$$\tilde{y}_s = \frac{k_{s1}k_{s2}\tilde{x}_{r1} - k_{s1}k_{s2}\tilde{x}_{r2} - k_{s2}\tilde{y}_{r1} + k_{s1}\tilde{y}_{r2}}{k_{s1} - k_{s2}}. \tag{21}$$

Because of the altering curvature of the reaction front, the downstream behavior of the Mach waves originated from adjacent points on the reaction front can be categorized into three situations, depending on the temperature distribution $\tilde{T}_e(\tilde{y})$, as schematically presented in Fig. 5. The method considers pairs of points on the reaction front to define the induced shock serves as a heuristic framework to capture the essential mechanism of induced shock formation. It is recognized that the actual physics underlying shock wave involves a continuous distribution of pressure waves generated along the reaction front, which may converge or diverge depending on local conditions.

For a steep temperature profile at the entrance, Fig. 5(a) shows that the pair of Mach waves produced at R_1 and R_2 may diverge as they propagate downstream. In this situation, the pair of compressing Mach waves cannot merge and thus fails to form a shock wave. For moderate slopes of temperature profiles at the entrance, the pair of compressing Mach waves propagates in a convergent manner, as indicated in Figs. 5(b) and 5(c). The presence of a crossing point, given by Eqs. (20) and (21), suggests the formation of a shock wave downstream of the reaction front, i.e., $\tilde{x}_s > \tilde{x}_{r2}$ and $\tilde{y}_s > \tilde{y}_{r2}$. Nevertheless, the appearance of a shock wave is the only necessary condition for detonation initiation. When the shock wave induced by Mach waves appears to be nearly parallel, the collapse resides too far away from the source points R_1 and R_2, such as the situation shown in Fig. 5(b). In such a situation, it is difficult to establish effective coupling between the shock wave and the reaction front connecting R_1 and R_2, and thereby, detonation initiation can hardly take place. Therefore, only thermal nonuniformity characterized by appropriate temperature profiles can lead to compressing Mach waves collapsing close to the reaction front, as indicated in Fig. 5(c), which exhibits a strong tendency to form a shock wave and to induce detonation initiation.

The inclined angle of the reaction front α_R varies with $\tilde{y}$. Specifically, there exists a threshold inclined angle $\alpha_{R,\mathrm{cr}}$ comparable with the Mach angle α_M. For large $|d\tilde{T}_e/d\tilde{y}|$, the reaction front has a small, inclined angle, i.e., $\alpha_R < \alpha_{R,\mathrm{cr}}$, resulting in the diverging Mach wave pair as shown in Fig. 5(a). In such a situation, no shock wave is generated downstream, and thereby, no detonation initiation happens. For small $|d\tilde{T}_e/d\tilde{y}|$, the inclined angle α_R is considerably greater than $\alpha_{R,\mathrm{cr}}$. As a result, Fig. 5(b) shows that the Mach wave pair converges at a large distance from the reaction front. However, strong interplay between the reaction front and the induced shock wave cannot be established. Therefore, detonation initiation can hardly take place. Only for intermediate $|d\tilde{T}_e/d\tilde{y}|$ does the reaction front satisfy $\alpha_R \gtrsim \alpha_{R,\mathrm{cr}}$, which produces a converging Mach wave near the reaction

front as shown in Fig. 5(c), and accordingly, it provides a favorable condition for detonation initiation.

For quantitative description, it requires a characteristic pairwise distance, denoted by $\tilde{d}_{\text{pair}}$, to build the correlation between the reaction front and its generated shock wave. For uniform temperature distribution at the inlet, the reaction front is strictly normal to the streamwise direction, and the Mach waves emitted from the reaction front are parallel to each other. Consequently, a shock wave cannot be produced, and thereby, detonation initiation does not happen. Therefore, the thermal nonuniformity imbedded in the supersonic reactive plays a decisive role in detonation initiation. In accordance, we may adopt the spatial dimension of the thermal nonuniformity as the characteristic pairwise distance, i.e., $\tilde{d}_{\text{pair}} = 1.0$.

The preceding discussion based on the Mach wave generation at sample points R_1 and R_2 provides a heuristic description, which can be generalized to multiple points. Statistically, we may select a sample of points on the reaction front, whose transverse coordinates are uniformly distributed. By discretizing the reaction front into sample points and examining the behavior of Mach waves originating from these points, we aim to capture the key mechanisms leading to shock formation, specifically the collapse of simple Mach waves as described by compressible fluid dynamics [52]. This statistical treatment provides a phenomenological insight that helps bridge the gap between theoretical descriptions and observed behaviors concerning the complex interactions between the reaction front and the induced shock wave.

For high accuracy in statistical analysis, the sample size should be sufficiently large. Accordingly, we set the point number to be $N = 10^4$. We have verified that the general results derived from the statistical analysis no longer change as N further increases. The induced shock wave is formed by sequential coalescence of Mach waves originated from the sample points on the reaction front. The coordinates for the sample points are $R_i = (\tilde{x}_{ri}, \tilde{y}_{ri})$, with $i = 1, 2, \ldots, N$, and the reaction front is discretized into $N - 1$ segments. According to the preceding discussion, each segment on the reaction front can produce a pair of Mach waves. Depending on the curvature of the reaction front, the Mach waves may either diverge or converge as they propagate downstream. The shock-inducing segment of the reaction front is defined such that it emits converging Mach waves. The summation of the shock-inducing segment constitutes the shock-inducing interval of the reaction front, denoted by $L_{\text{sh-in}}$. The simplified model in this paper offers qualitative insights into how the temperature gradient, identified by thermal nonuniformity, affects the geometry of reaction fronts in the supersonic reactive flow field. Despite that the simplified model may not fully capture all details of shock-reaction front interactions, it provides elementary understandings on the self-strengthening mechanism between the induced shock wave and the reaction front, leading to detonation initiation.

Analyzing the distribution of the shock-inducing segment on the reaction front, we may define a column vector $I_{\text{sh-in}}$ with a unit element corresponding to the index of shock-inducing segments on the reaction front and zero element corresponding to the rest of the segments. Summing all elements in the column vector $I_{\text{sh-in}}$ gives the total number of the shock-inducing segments, which is denoted by $N_{\text{sh-in}}$. In analogy to the discretization of the reaction front, the induced shock wave can be represented by the $N_{\text{sh-in}}$ points and $N_{\text{sh-in}} - 1$ segments connecting the adjacent points. The ratio $\eta_{\text{sh-in}} = N_{\text{sh-in}}/N$ measures the effectiveness of the reaction front in producing shock waves. A higher value of $\eta_{\text{sh-in}}$ means that more segments on the reaction front contribute to shock formation and thereby facilitate detonation initiation. Nevertheless, the induced shock wave may extend remotely, where it can hardly facilitate the chemical reaction and thus makes little contribution to detonation initiation. Therefore, it requires spotting the portion of the reaction front that is sufficiently close to the induced shock wave to establish its synergistic interaction leading to detonation initiation. After discretization, the geometric characteristics of both the reaction front and the induced shock wave can be represented by N and $\eta_{\text{sh-in}}$ separate points, respectively. The pairwise distance between individual points on the reaction front and the induced shock wave can be cast into the matrix $\mathbf{S}$. The element s_{mn} of the matrix $\mathbf{S}$ refers to the distance between the point with index m on the reaction and the point with index n on the induced shock wave.
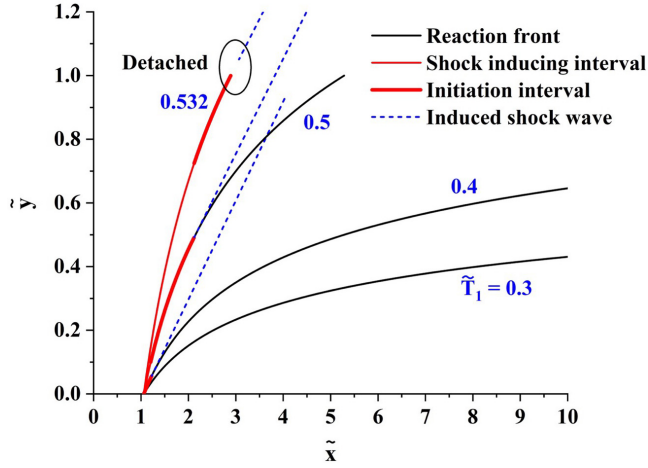
FIG. 6. The distributions of reaction front and its induced shock wave in the supersonic reactive flow field with different upper boundary temperatures, i.e., $\tilde{T}_1 = 0.3$, $\tilde{T}_1 = 0.4$, $\tilde{T}_1 = 0.5$, and $\tilde{T}_1 = 0.532$. Note that we fix $\tilde{T}_e(\tilde{y} = 0) = \tilde{T}_0 = 0.6$ and only change the value of $\tilde{T}_e(\tilde{y} = 1) = \tilde{T}_1$.

With knowledge of the pairwise distance matrix $\mathbf{S}$, we define the initiation segments on the reaction front by selecting row vectors of the matrix $\mathbf{S}$, which contains at least one element s_{ij} smaller than the characteristic distance, i.e., $s_{ij} < \tilde{d}_{\text{pair}}$. All initiation segments compose the initiation interval on the reaction front, denoted by $L_{\text{initiation}}$. In analogy to $I_{\text{sh-in}}$, we can introduce an additional index column vector $I_{\text{initiation}}$ with a unit element corresponding to the initiating segment on the reaction front and zero element corresponding to other segments.

Figure 6 shows that the overall curvature of the reaction front becomes smaller for higher temperature at the upper boundary (i.e., smaller temperature gradient of the thermal nonuniformity). With the help of the index vector $I_{\text{sh-in}}$, the shock-inducing interval, and the induced shock wave are respectively denoted by the red solid lines and blue dashed lines in Fig. 6. By means of the index vector $I_{\text{initiation}}$, we can determine the initiation interval, which contributes to shock wave formation and meanwhile participates in the synergistic feedback. The initiation interval plays a decisive role in detonation initiation and is represented by the thickened red lines.

The results in Fig. 6 indicate that the shock-inducing interval becomes longer for higher $\tilde{T}_1$. This is because the streamwise bending of the reaction reduces when $\tilde{T}_1$ increases. This phenomenon can be examined with the help of the critical inclined angle of the reaction front. As $\tilde{T}_1$ increases, the inclined angle of each segment on the reaction front grows larger, whereas the value of the critical inclined angle $\alpha_{R,\text{cr}}$ hardly changes with $\tilde{T}_1$. Therefore, higher $\tilde{T}_1$ corresponds to a larger proportion of the reaction front that should be incorporated into the shock-inducing interval. Interestingly, it is observed that the shock-inducing interval and the initiation interval no longer coincide for $\tilde{T}_1 = 0.50$. This is explained as follows. The transverse elevation corresponding to $\alpha_{R,\text{cr}}$ increases with $\tilde{T}_1$, and thereby the induced shock wave appears with a larger transverse coordinate. The distance between the lower boundary to the induced shock wave exceeds the characteristic length $\tilde{d}_{\text{pair}}$, and thus, the proportion of the reaction close to $\tilde{y} = 0$ should be excluded from the initiation interval. When $\tilde{T}_1$ becomes sufficiently high, Fig. 6 shows that the shock-inducing interval spreads over the whole reaction front, whereas the induced shock wave becomes detached from the reaction front. In this situation, the initiation interval rapidly shrinks and finally vanishes when the distance between the induced shock wave and the reaction front exceeds $\tilde{d}_{\text{pair}}$. This indicates that detonation can hardly be initiated when the magnitude of the temperature gradient becomes too small.

The inner product of the index vectors $I_{\text{sh-in}}$ and $I_{\text{initiation}}$ gives the total number of segments on the reaction front that both lead to shock wave generation and meanwhile participate in the synergistic
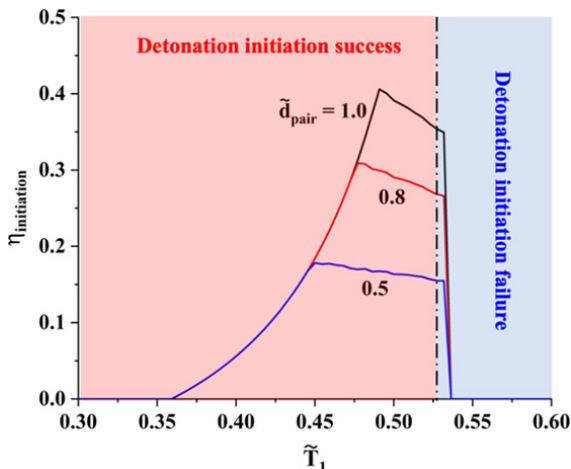
FIG. 7. Change of the detonation initiation factor $\eta_{\text{initiation}}$, with temperature at upper boundary $\tilde{T}_1$ for different values of $\tilde{d}_{\text{pair}}$. Numerical simulation shows that detonation initiation succeeds when $\tilde{T}_1 < 0.525$ (i.e., the vertical dashed line).

feedback with the induced shock wave. Consequently, we may define an initiation factor $\eta_{\text{initiation}}$ in terms of index vectors $I_{\text{sh-in}}$ and $I_{\text{initiation}}$, i.e.,

$$\eta_{\text{initiation}} = \frac{I_{\text{sh-in}} I_{\text{initiation}}}{N}. \tag{22}$$

The initiation factor $\eta_{\text{initiation}}$ represents the proportion of the reaction front that helps to induce detonation initiation and thus quantifies the capability of the thermal uniformity causing detonation initiation.

Figure 7 indicates that, for linear temperature distribution with fixed temperature of $\tilde{T}_0 = 0.6$ at the lower boundary, the initiation factor changes nonmonotonically with $\tilde{T}_1$ at the upper end. As the upper boundary temperature increases from the normal value of $\tilde{T}_1 = 0.30$ (i.e., $T_1 = 600$ K), there exist sequentially the detonation initiation enhancing regime (with $\tilde{T}_1$ ranging from 0.36 to 0.46), the detonation initiation saturation regime (with $\tilde{T}_1$ ranging from 0.46 to 0.53), and the detonation initiation failure regime (with $\tilde{T}_1$ beyond 0.54, which is very close to $\tilde{T}_0$). Transition between those regimes is characterized by substantial change in detonation initiation factor.

At the initiation enhancing regime, the strong bending of the reaction front substantially shortens the shock-inducing interval on the reaction front and thereby reduces the intensity of the induced shock wave. When $\tilde{T}_1$ increases, the curvature of the reaction front decreases, and accordingly, the shock-inducing interval grows, intensifying the shock wave. At such situations, the initiation interval coincides with the shock-inducing interval, resulting in the increase of the initiation factor $\eta_{\text{initiation}}$. At some intermediate value of $\tilde{T}_1$, the initiation factor reaches its peak value, which defines the most favorable situation for detonation initiation. After the peak value of $\eta_{\text{initiation}}$, the initiation saturation regime appears. As $\tilde{T}_1$ further increases, the initiation factor moderately reduces and then rapidly falls to zero as $\tilde{T}_1$ reaches beyond some critical value. The moderate reduction of $\eta_{\text{initiation}}$ can be understood as follows. At moderate to high value of $\tilde{T}_1$, the initiation interval tends to detach from the lower boundary, e.g., $\tilde{T}_1 = 0.532$ shown in Fig. 6. Despite continuous increasing of the shock-inducing interval with $\tilde{T}_1$, the proportion of the initiation interval on the reaction front reduces due to the transverse elevation of the induced shock wave. At sufficiently high values of $\tilde{T}_1$, the reaction front and the indued shock wave move apart, which significantly reduces the possibility of detonation initiation. The initiation failure regime is characterized by rapidly shortening and finally vanishing of the initiation interval.

In the preceding discussion, the characteristic pairwise distance is specified to be the spatial dimension of the thermal nonuniformity, i.e., $\tilde{d}_{\text{pair}} = 1.0$. Adopting shorter $\tilde{d}_{\text{pair}}$ promotes the standard in defining the initiation interval on the reaction front. Therefore, Fig. 7 shows that the peak value of $\eta_{\text{initiation}}$ drops significantly when $\tilde{d}_{\text{pair}}$ decreases. Nevertheless, the general characteristics of the variation of $\eta_{\text{initiation}}$ with $\tilde{T}_1$ only change slightly for different characteristic pairwise distances. Numerical simulation results on detonation initiation are indicated by the semitransparent domains in Fig. 7, in which the red domain denotes the regime of detonation initiation success, and the blue domain refers to detonation initiation failure. Though the simulation results are not the same as theoretical prediction, reasonable agreement is still achieved. Both theory and simulation show that detonation initiation fails when the upper boundary temperature approaches that at the lower boundary, i.e., the thermal nonuniformity becomes sufficiently weak. Numerical simulation shows that detonation initiation succeeds when $\tilde{T}_1 < 0.525$, which is lower than the threshold value predicted by the theoretical model.

The physical significance of detonation initiation factor $\eta_{\text{initiation}}$ can be substantiated by aligning with our recent numerical studies [53], which examined the relationship between reaction front propagation speeds and the Chapman-Jouguet (CJ) speed under varying temperature gradients. In that numerical simulation, three regimes for detonation initiation were identified. At low-temperature gradient regime, the speed of the autoignition driven reaction front is much faster than the local sound speed, and the pressure waves induced by heat release can hardly converge ahead of the reaction zone, which aligns with the initiation failure regime presented by the current model. At the moderate-temperature gradient regime, the local autoignition-driven reaction front induces a series of pressure waves. Positive feedback occurs between the reaction front and the induced pressure waves, resulting in the self-strengthening effect and thus detonation initiation, which aligns with the initiation saturation regime predicted by the current theoretical model. At the high-temperature gradient, the correlation between the reaction front and the induced pressure intensifies with reducing the temperature gradient, which corresponds to the initiation enhancing regime. These findings demonstrate that the trends observed in the numerical simulations are consistent with our theoretical results, highlighting the critical role of the temperature gradient in controlling the detonation initiation process. By introducing the initiation factor $\eta_{\text{initiation}}$, our model provides a qualitative measure that aligns with numerical results and captures the variability in detonation tendencies under different thermal conditions, reinforcing the theoretical explanations presented in this paper.

In the above discussion, we only consider the linear temperature distribution at the inlet. In general, the temperature profile of the thermal nonuniformity exhibits as either upward convex with $\alpha_T > 1$ or downward convex with $\alpha_T < 1$. For the given intensity of thermal nonuniformity, i.e., fixed $\tilde{T}_1$ and $\tilde{T}_0$, the reaction front corresponding to various α_T's coincides at both upper and lower boundaries as compared in Fig. 8(a) for $\alpha_T = 0.5$ and 1.0. However, the strength of the streamwise bending of the reaction front depends on the factor α_T.

Figure 8 compares the reaction front (thin black line), the shock inducing interval (think red line), the initiation interval (thickened red line), and the induced shock wave (blue dashed line) at various temperature profile factors α_T. An interesting phenomenon occurs for temperature distribution with $\alpha_T = 0.5$. The downward convexity of the temperature profile leads to rapid increase in the reaction length and makes the reaction front downward convex [see Fig. 8(a)]. Such a geometric characteristic of the reaction front exhibits twofold impacts on the detonation results. For moderate $\tilde{T}_1$, Fig. 8(a) shows that the intensified bending of the reaction front inhibits the generation of a shock wave for $\tilde{T}_1 = 0.50$, and thus, detonation initiation can hardly take place. However, for sufficiently high $\tilde{T}_1$, the downward convexity of the reaction front near the lower boundary provides suitable conditions to induce an additional branch of a shock wave, as indicated by the blue dashed line for $T_1 = 0.55$ in Fig. 8(a). This additional induced shock wave remains close to the reaction front for the downward convex temperature profile with $\alpha_T = 0.55$. Figure 8(a) shows that this additional induced shock wave produces a substantially longer initiation interval than that for the linear temperature profile with $\alpha_T = 1.0$.
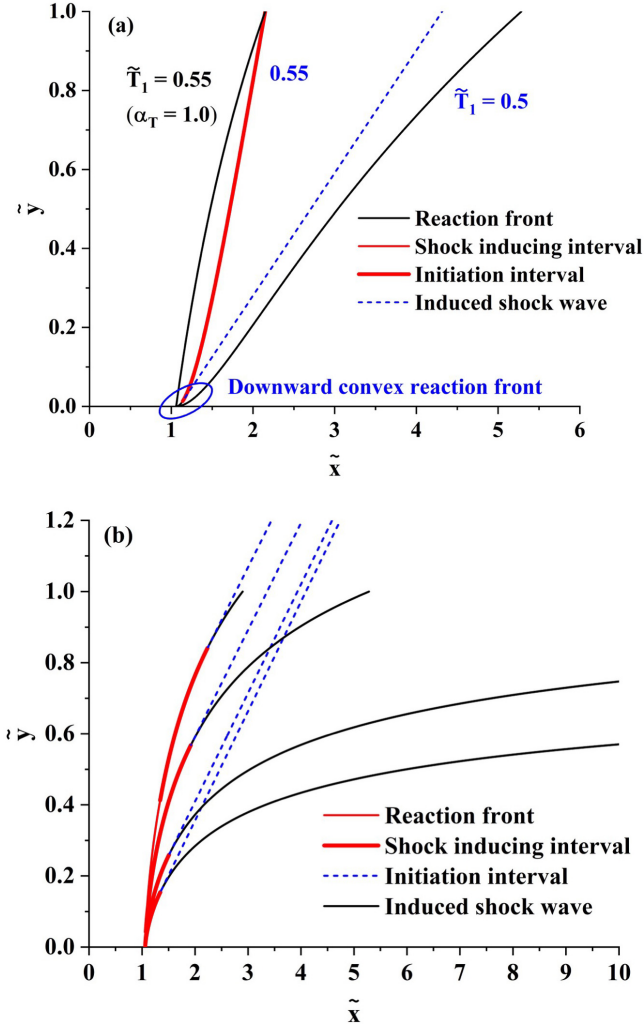
FIG. 8. Comparison of the reaction fronts corresponding to different temperature distributions at the inlet for (a) $\alpha_T = 0.5$ (downward convex $\tilde{T}_e$) and (b) $\alpha_T = 1.5$ (upward convex $\tilde{T}_e$). Note that we fix $\tilde{T}_e(\tilde{y} = 0) = \tilde{T}_0 = 0.6$ and change $\tilde{T}_e(\tilde{y} = 1) = \tilde{T}_1$ and α_T. The reaction front, initiation interval, and induced shock waves are represented by the thin black line, thickened red line, and dashed blue line, respectively.

Comparing Fig. 8(b) with Fig. 6 indicates that the initiation interval on the reaction front is greatly extended when the thermal nonuniformity has an upward convex temperature distribution (i.e., $\alpha_T = 1.5$). For instance, the induced shock wave is detached at situations with $\tilde{T}_1 = 0.532$ for the linear temperature profile ($\alpha_T = 1.0$), while it becomes attached to the reaction front when the temperature profile changes to be upward convex ($\alpha_T = 1.5$), and moreover, the initiation interval is substantially lengthened. Such a phenomenon can be attributed to slower temperature reduction close to the lower boundary with $\tilde{y} = 0$ for $\alpha_T = 1.5$ in comparison with that for $\alpha_T = 1.0$. The reaction front corresponding to the upward convex temperature profile tends to be more normal to the lower boundary. Such a profile of the reaction front facilitates the generation of an induced shock wave as well as the lengthening of the initiation interval.

Figure 9 shows that the initiation factor for thermal nonuniformity with an upward convex temperature profile ($\alpha_T = 1.5$) is consistently higher than that for the linear temperature profile
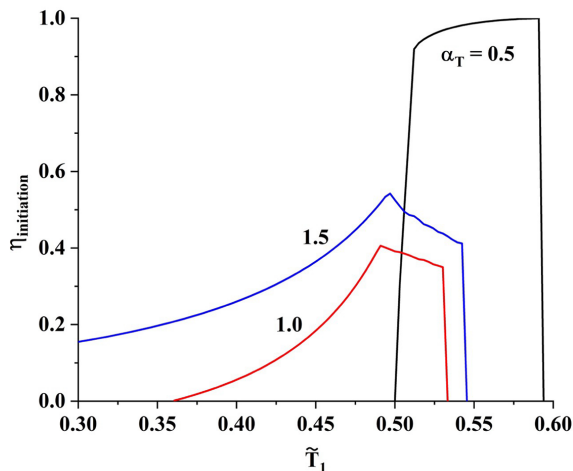
FIG. 9. Change of the detonation initiation factor $\eta_{\text{initiation}}$, with temperature at upper boundary $\tilde{T}_1$ for different values of α_T. The lower boundary temperature is fixed to be $\tilde{T}_0 = 0.6$.

($\alpha_T = 1.0$). It suggests that thermal nonuniformity with an upward convex temperature distribution has stronger capability in causing detonation initiation than that with a linear distribution. An interesting phenomenon occurs for thermal nonuniformity with a downward temperature profile ($\alpha_T = 0.5$), which generates a reaction front having downward convexity close to the lower bound at $\tilde{y} = 0$. Such a geometric characteristic of the reaction front exhibits twofold impacts on the detonation results. For low to moderate $\tilde{T}_1$, the intensified streamwise bending of the reaction front exceedingly inhibits shock wave formation, and thus, detonation initiation can hardly take place. However, for relatively high $\tilde{T}_1$, the downward convex reaction front near $\tilde{y} = 0$ provides suitable conditions to induce an additional shock wave branch, see the blue dashed line in Fig. 8(a). This induced shock wave remains close to the reaction front and thus substantially facilitates detonation initiation, particularly for thermal nonuniformity with small temperature difference. Figure 9 shows that $\eta_{\text{initiation}}$ for the downward convex temperature profile ($\alpha_T = 0.5$) is highly peaked in a regime with $T_1 \lesssim T_0$.

IV. TWO-DIMENSIONAL ANALYSIS ON DETONATION INITIATION

A. Revised reaction front

In Sec. III, the supersonic reactive flow is assumed to be one dimensional, and the reaction fronts and induced shock waves are derived by regarding the transverse coordinate as a parameter. However, the pressure wave can induce convection in the transverse direction, which enhances the thermal energy exchange between fluid elements with different transverse coordinates. Consequently, the fluid element at a large transverse coordinate receives additional energy supply before autoignition takes place. Therefore, the transverse convection tends to shorten the reaction length at larger $\tilde{y}$ and thus reduces the streamwise bending of the reaction front.

The preceding discussion demonstrates that the geometric characteristics of the reaction front plays a crucial role in detonation initiation. Therefore, a more rigorous approach dealing with the thermal nonuniformity embedded in supersonic reactive flow must consider the effect of two-dimensional flow field. The governing equations are revised by including the convective heat and mass transfer in the transverse direction, i.e.,

$$\frac{\partial \tilde{T}}{\partial \tilde{x}} + \tilde{v}\frac{\partial \tilde{T}}{\partial \tilde{y}} = \tilde{B}\tilde{c}_F \exp\left(-\frac{\tilde{T}_a}{\tilde{T}}\right), \tag{23}$$

$$\frac{\partial \tilde{c}_F}{\partial \tilde{x}} + \tilde{v}\frac{\partial \tilde{c}_F}{\partial \tilde{y}} = -\tilde{B}\tilde{c}_F \exp\left(-\frac{\tilde{T}_a}{\tilde{T}}\right), \tag{24}$$

where $\tilde{v} = v/U$ is the nondimensional transverse velocity induced by chemical heat release. The conserved quantity $\beta = \tilde{T} + \tilde{c}_F$ now satisfies

$$\frac{\partial \beta}{\partial \tilde{x}} = -\tilde{v}\frac{\partial \beta}{\partial \tilde{y}}. \tag{25}$$

Before autoignition, the uniform concentration of the combustible mixture remains almost unchanged, i.e., $\tilde{c}_F = 1$, implying that the transverse variation of β is characterized by the temperature gradient there, i.e., $d\beta/d\tilde{y} \sim d\tilde{T}/d\tilde{y}$. For highly supersonic flow, i.e., $U \gg a_e$, the transverse velocity induced by the pressure wave should be much smaller than the streamwise component, i.e., $\tilde{v} \ll 1$. Preceding to autoignition, we assume that the temperature gradient has little change from that at the entrance, i.e.,

$$\frac{d\tilde{T}}{d\tilde{y}} \sim \frac{d\tilde{T}_e}{d\tilde{y}} \sim O(1). \tag{26}$$

Substituting $\tilde{v} \ll 1$ and $d\beta/d\tilde{y} \sim O(1)$ into Eq. (25), one obtains $\partial\beta/\partial\tilde{x} \ll 1$. This suggests that the correlation between $\tilde{c}_F$ and $\tilde{T}$, given by Eq. (13), can also be adopted in the two-dimensional situation. Substituting Eq. (13) into Eq. (25), we have

$$\frac{\partial \tilde{T}}{\partial \tilde{x}} = \tilde{B}(1 + \tilde{T}_e - \tilde{T})\exp\left(-\frac{\tilde{T}_a}{\tilde{T}}\right) - \tilde{v}\frac{\partial \tilde{T}}{\partial \tilde{y}}. \tag{27}$$

In analogy to Eq. (15), the reaction length can be determined in the following form:

$$\tilde{L}'_{\text{reaction}} = \int_{\tilde{T}_e}^{1+\tilde{T}_e} \frac{d\tilde{T}}{\tilde{B}(1 + \tilde{T}_e - \tilde{T})\exp(-\tilde{T}_a/\tilde{T}) - \tilde{v}\partial\tilde{T}/\partial y}. \tag{28}$$

The evaluation of the integral on the right-hand side of Eq. (28) requires the knowledge of the transverse velocity $\tilde{v}$, the temperature gradient $\partial\tilde{T}/\partial\tilde{y}$, and their dependence on nondimensional temperature by means of Eq. (14).

Equation (28) introduces an additional term to account for the transverse convection effects, which are absent in Eq. (15). This additional term arises due to the convective transport of heat and species in the transverse direction, induced by the perturbation pressure generated by chemical heat release. The inclusion of this term in Eq. (28) reveals how transverse convection can affect the local temperature distribution and, consequently, the geometry of the reaction front. This impact is particularly pronounced in regions with higher transverse temperature gradients. When the transverse velocity component is considered, the reaction length is shortened in regions with strong transverse temperature gradients, as the enhanced convective heat transfer facilitates quicker energy redistribution. The two-dimensional model captures this effect, showing that transverse convection promotes or inhibits detonation initiation depending on the strength and profile of the thermal nonuniformity. The revised reaction front given by Eq. (28) demonstrates that, for weak thermal nonuniformity, transverse convection may hinder detonation initiation by reducing the coupling between the induced shock wave and the reaction front. Conversely, in cases of strong thermal nonuniformity, the additional transverse convection term can enhance the initiation by intensifying the shock-reaction front interaction.

B. Perturbation pressure due to chemical heat release

In terms of uniform flow velocity U and streamwise coordinate x, a conceptual time τ could be introduced in the steady flow field, i.e., $\tau = x/U$. The conceptual time can be regarded as the progress variable measuring the chemical reaction process, and its nondimensional form is

$\tilde{\tau} = (x/U)/(h/U) = x/h$. Tracking the motion of a fluid element in such a reactive flow field, its temperature and included reactant concentration satisfy

$$\frac{d\tilde{T}}{d\tilde{\tau}} = \tilde{B}\tilde{c}_F \exp\left(-\frac{\tilde{T}_a}{T}\right), \quad \frac{d\tilde{c}_F}{d\tilde{\tau}} = -\tilde{B}\tilde{c}_F \exp\left(-\frac{\tilde{T}_a}{\tilde{T}}\right), \tag{29}$$

where the differential operator d shall be regarded as a substantial derivative. According to Rayleigh's criterion, the onset of chemical reaction induces an unsteady heat addition in the fluid element, which generates pressure waves propagating outwardly. The pressure is nondimensionalized by the momentum flux of the uniform stream $\tilde{p} = p/\rho_0 U^2$, where ρ_0 is the density of the reactive fluid at the inlet with $\tilde{y} = 0$. The amplitude of the pressure wave depends on the variation of the heat release rate during the chemical reaction process. Observing the pressure wave characteristics on the moving fluid element, the governing equation can be written in the following form [45]:

$$\frac{\partial^2 \tilde{p}}{\partial \tilde{\tau}^2} - \frac{1}{M^2}\tilde{\nabla}^2 \tilde{p} = (\gamma - 1)\frac{d^2 \tilde{q}}{d\tilde{\tau}^2}, \tag{30}$$

where $\gamma = c_p/c_v$ is the heat capacity ratio, and $\tilde{q} = q/\rho_0 U^2$ the nondimensional volumetric heat release from chemical reaction. The use of Eq. (30) is intended to provide a first-order analytical approximation of the pressure perturbation in the reactive supersonic flow. We recognize that varying the speed of sound introduces complexities which need more rigorous treatments in mathematics. However, this theoretical model aims to underline the interaction mechanism between the compression wave and the reaction front rather than a comprehensive solution that accounts for all variations.

In Cartesian coordinates, the nondimensional Laplace operator can be written as

$$\tilde{\nabla}^2 \tilde{p} = \frac{\partial^2 \tilde{p}}{\partial \tilde{x}^2} + \frac{\partial^2 \tilde{p}}{\partial \tilde{y}^2}, \tag{31}$$

where the coordinates $\tilde{x}$ and $\tilde{y}$ refer to the relative distance from the observing fluid element. In terms of the conceptual time, the derivative with respect to the streamwise coordinate can be converted into the following alternative form:

$$\frac{\partial^2 \tilde{p}}{\partial \tilde{x}^2} = \frac{\partial^2 \tilde{p}}{\partial \tilde{\tau}^2}. \tag{32}$$

Substituting Eqs. (31) and (32) into Eq. (30) yields

$$\frac{\partial^2 \tilde{p}}{\partial \tilde{\tau}^2} - \frac{1}{M^2 - 1}\frac{\partial^2 \tilde{p}}{\partial \tilde{y}^2} = \frac{(\gamma - 1)M^2}{M^2 - 1}\frac{d^2 \tilde{q}}{d\tilde{\tau}^2}. \tag{33}$$

Equation (33) describes an effective one-dimensional pressure wave propagating in the transverse direction. The initial conditions of Eq. (33) shall be determined by the state of fluid at the inlet, where the pressure wave has not been produced due to negligible chemical reaction. Therefore, we may write

$$\tilde{p} = 0 \quad \text{and} \quad \frac{\partial \tilde{p}}{\partial \tilde{\tau}} = 0 \quad \text{at } \tilde{\tau} = 0. \tag{34}$$

The physical meaning of Eq. (33) can be underlined as follows. In supersonic flow, the pressure wave can propagate only in the downstream direction. Accordingly, the pressure wave domain can be defined as a particular field region outside which the pressure wave exhibits no effects on the supersonic flow. The angle between the boundary of the pressure wave domain and the supersonic flow direction is identical to the Mach angle α_M, which satisfies $\alpha_M = \arcsin(1/M)$. For reactive flow, the states in the fluid element change during its motion at constant speed. By means of the conceptual time, such behavior can be interpreted as the unsteady variation of the states in the concerned fluid element. Therefore, the steady two-dimensional Mach line in $\tilde{x}$-$\tilde{y}$ space can
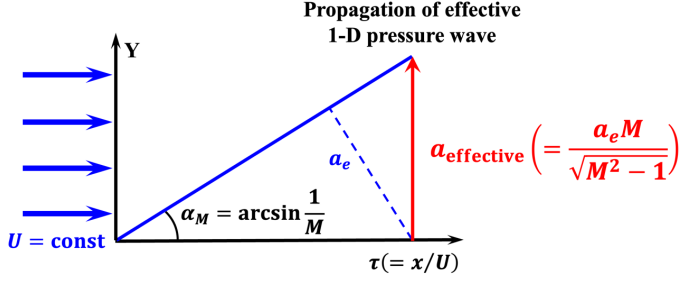
FIG. 10. Schematic for the propagation of the effective one-dimensional pressure in the phase space expanded by conceptual time and transverse coordinate space.

be regarded as an effective unsteady one-dimensional wave in temporal-spatial space generated by conceptual time and transverse coordinates. Figure 10 shows the schematic of this effective unsteady one-dimensional wave. Comparing Eqs. (30) and (33), the effective propagation speed of this one-dimensional pressure wave correlates to the acoustic speed through $a_{\text{effective}} = a_e M/\sqrt{M^2-1}$.

The analytical solution of Eq. (33) subject to the initial conditions in Eq. (34) can be written in the following form:

$$\tilde{p} = \frac{(\gamma-1)M^2}{2\sqrt{M^2-1}} \int_0^{\tilde{\tau}} \int_{\tilde{y}-\frac{1}{\sqrt{M^2-1}}(\tilde{\tau}-\tilde{\tau}')}^{\tilde{y}+\frac{1}{\sqrt{M^2-1}}(\tilde{\tau}-\tilde{\tau}')} \frac{d^2\tilde{q}}{d\tilde{\tau}^2} d\tilde{y}' d\tilde{\tau}'. \tag{35}$$

To evaluate the integrals on the right-hand side of Eq. (35), we need to evaluate the rate of chemical heat release $d^2\tilde{q}/d\tilde{\tau}^2$. The chemical heat release results from the conversion of the reactant to a product, and its rate is proportional to that of reactant depletion, i.e.,

$$\frac{d\tilde{q}}{d\tilde{\tau}} = -\tilde{Q}\frac{d\tilde{c}_F}{d\tilde{\tau}}, \tag{36}$$

where $\tilde{Q} = Q/(\rho_0 U^2/c_{F0})$ is the nondimensional molar heat release due to chemical reaction. The derivative $d\tilde{c}_F/d\tilde{\tau}$, according to Eq. (13) is equivalent to $-d\tilde{T}/d\tilde{\tau}$. Therefore, the inhomogeneous term on the right-hand side of Eq. (33) can be determined as

$$\frac{d^2\tilde{q}}{d\tilde{\tau}^2} = \tilde{Q}\frac{d^2\tilde{T}}{d\tilde{\tau}^2} = \tilde{Q}\tilde{B}^2\tilde{T}_a \exp\left(-\frac{2\tilde{T}_a}{\tilde{T}}\right)\left(\frac{1+\tilde{T}_e}{\tilde{T}}-1\right)^2, \tag{37}$$

where we have used a large activation temperature $\tilde{T}_a \gg \tilde{T}$.

Substituting Eq. (37) into Eq. (35) and noticing that the spatial coordinate y does not appear in Eq. (36) explicitly, the pressure field induced by the compression wave can be written as

$$\tilde{p} = \frac{(\gamma-1)M^2}{(M^2-1)} \tilde{Q}\tilde{B}^2\tilde{T}_a \int_0^{\tilde{\tau}} (\tilde{\tau}-\tilde{\tau}') \exp\left(-\frac{2\tilde{T}_a}{\tilde{T}}\right)\left(\frac{1+\tilde{T}_e}{\tilde{T}}-1\right)^2 d\tilde{\tau}'. \tag{38}$$

Using integration by parts, the term $(\tau-\tau')$ could be converted into an additional fold of integration. Accordingly, Eq. (38) can be written in an alternative form:

$$\tilde{p} = \frac{(\gamma-1)M^2}{(M^2-1)} \tilde{Q}\tilde{B}^2\tilde{T}_a \int_0^{\tilde{\tau}} \int_0^{\tilde{\tau}'} \exp\left(-\frac{2\tilde{T}_a}{\tilde{T}}\right)\left(\frac{1+\tilde{T}_e}{\tilde{T}}-1\right)^2 d\tilde{\tau}'' d\tilde{\tau}'. \tag{39}$$

Recalling the definition of conceptual time, the integration with respect to $\tilde{\tau}$ is equivalent to that with respect to streamwise coordinate $\tilde{x}$. Using Eq. (14), the integral variable can be further replaced by nondimensional temperature $\tilde{T}$. According to Eq. (11), the magnitude of $\tilde{T}$ in a fluid element increases by unity from the unburnt to the burnt state. This suggests that the streamwise variation

of nondimensional temperature should satisfy $\partial \tilde{T}/\partial \tilde{x} \sim O(1)$. Combining the scaling relation for transverse variation of $\tilde{T}$ given by Eq. (26) and recalling that $v \ll U$, Eq. (14) can be approximated as

$$\frac{d\tilde{x}}{d\tilde{T}} \approx \frac{\exp(\tilde{T}_a/\tilde{T})}{\tilde{B}(1 + \tilde{T}_e - \tilde{T})}. \tag{40}$$

With the help of Eq. (40) and evaluating the integral involving exponential terms $\exp(-\tilde{T}_a/\tilde{T})$ in the asymptotic sense, the inner integral can be evaluated as

$$\int_0^{\tilde{\tau}'} \exp\left(-\frac{2\tilde{T}_a}{\tilde{T}}\right)\left(\frac{1 + \tilde{T}_e}{\tilde{T}} - 1\right)^2 d\tilde{\tau}''$$

$$= \int_0^{\tilde{x}'} \exp\left(-\frac{2\tilde{T}_a}{\tilde{T}}\right)\left(\frac{1 + \tilde{T}_e}{\tilde{T}} - 1\right)^2 d\tilde{x}'' = \frac{1}{\tilde{B}}\int_{\tilde{T}_o}^{\tilde{T}'} \frac{1 + \tilde{T}_e - \tilde{T}}{\tilde{T}^2} \exp\left(-\frac{\tilde{T}_a}{\tilde{T}}\right) d\tilde{T}$$

$$\approx \frac{1 + \tilde{T}_e - \tilde{T}'}{\tilde{B}\tilde{T}_a} \exp\left(-\frac{\tilde{T}_a}{\tilde{T}}\right). \tag{41}$$

We have used the fact that $\exp[-\tilde{T}_a/(1 + \tilde{T}_0)] \gg \exp(-\tilde{T}_a/\tilde{T}_0)$, which holds for reaction involving large activation energy. Proceeding to the outer integration and converting the integral variable from $\tilde{x}$ to $\tilde{T}$ yields

$$\int_0^{\tilde{\tau}} \frac{(1 + \tilde{T}_e - \tilde{T}')}{B\tilde{T}_a} \exp\left(-\frac{\tilde{T}_a}{\tilde{T}'}\right) d\tau'$$

$$= \frac{1}{\tilde{B}\tilde{T}_a}\int_0^{\tilde{x}}(1 + \tilde{T}_e - \tilde{T}')\exp\left(-\frac{\tilde{T}_a}{\tilde{T}'}\right) d\tilde{x}' = \frac{1}{\tilde{B}^2\tilde{T}_a}\int_{\tilde{T}_e}^{\tilde{T}} d\tilde{T}' = \frac{\tilde{T} - \tilde{T}_e}{\tilde{B}^2\tilde{T}_a}. \tag{42}$$

Substituting Eqs. (41) and (42) into the twofold integral on the right-hand side of Eq. (39), we obtain

$$\tilde{p}(\tilde{x}, \tilde{y}) = \frac{(\gamma - 1)M^2(\tilde{y})}{M^2(\tilde{y}) - 1}\tilde{Q}\tilde{B}^2[\tilde{T}(\tilde{x}) - \tilde{T}_e(\tilde{y})], \tag{43}$$

which characterizes the perturbation pressure corresponding to the compression wave. For highly supersonic flow, e.g., $M > 3$, we have $M^2/(M^2 - 1) \approx 1$. Therefore, the perturbation pressure field in Eq. (39) is reduced to

$$\tilde{p}(\tilde{x}, \tilde{y}) = \tilde{Q}\tilde{B}^2(\gamma - 1)[\tilde{T}(\tilde{x}) - \tilde{T}_e(\tilde{y})]. \tag{44}$$

C. Transverse velocity induced by perturbation pressure

The gradient of the perturbation pressure has a nonvanishing component in the transverse direction, which leads to transverse velocity v in association with the uniform streamwise velocity U. This two-dimensional flow field satisfies continuity and Euler equations, which in steady state are written in the following nondimensional form:

$$\frac{\partial \tilde{\rho}}{\partial \tilde{x}} + \frac{\partial}{\partial \tilde{y}}(\tilde{\rho}\tilde{v}) = 0, \tag{45}$$

$$0 = -\frac{1}{\tilde{\rho}}\frac{\partial \tilde{p}}{\partial \tilde{x}}, \tag{46}$$

$$\frac{\partial \tilde{v}}{\partial x} + \tilde{v}\frac{\partial \tilde{v}}{\partial y} = -\frac{1}{\tilde{\rho}}\frac{\partial \tilde{p}}{\partial y}. \tag{47}$$

It shall be noted that the absence of streamwise velocity is due to the normalization process, which yields $\tilde{U} = 1$. Equation (46) results from the constancy of uniform velocity U. By means of the

chain rule, the partial derivative of $\tilde{v}$ and $\tilde{p}$ with respect to coordinates $\tilde{x}$ and $\tilde{y}$ can be converted into alternative forms:

$$\frac{\partial \tilde{v}}{\partial \tilde{x}} = \frac{\partial \tilde{v}}{\partial \tilde{T}} \frac{\partial \tilde{T}}{\partial \tilde{x}}, \quad \frac{\partial \tilde{v}}{\partial \tilde{y}} = \frac{\partial \tilde{v}}{\partial \tilde{T}} \frac{\partial \tilde{T}}{\partial \tilde{y}}, \quad \frac{\partial \tilde{p}}{\partial \tilde{y}} = \frac{\partial \tilde{p}}{\partial \tilde{T}} \frac{\partial \tilde{T}}{\partial \tilde{y}}. \tag{48}$$

Substituting Eq. (48) into (47), we obtain

$$\left(\frac{\partial \tilde{T}}{\partial \tilde{x}} + \tilde{v} \frac{\partial \tilde{T}}{\partial \tilde{y}} \right) \frac{\partial \tilde{v}}{\partial \tilde{T}} = -\frac{1}{\tilde{\rho}} \frac{\partial \tilde{p}}{\partial \tilde{T}} \frac{\partial \tilde{T}}{\partial \tilde{y}}. \tag{49}$$

Substituting Eq. (27) into (49) and multiplying v on both sides, the convective thermal transport in the transverse direction can be expressed as

$$-\tilde{v} \frac{\partial T}{\partial \tilde{y}} = \tilde{B}(1 + \tilde{T}_e - \tilde{T}) \exp\left(-\frac{\tilde{T}_a}{\tilde{T}} \right) \tilde{\rho} \frac{\partial}{\partial \tilde{p}} \left(\frac{\tilde{v}^2}{2} \right). \tag{50}$$

The transverse velocity originates from the pressure perturbation. Based on dimensional consideration, it may be constituted as

$$\tilde{v} = \alpha_v \sqrt{\frac{\tilde{p}}{\tilde{\rho}}}, \tag{51}$$

where α_v is a scaling factor to be determined.

Accurate evaluation of α_v requires solving the continuity Eq. (45) and the Euler Eqs. (46) and (47), which is of formidable difficulty in analysis. Nevertheless, the parameter α_v can be evaluated with approximation. Substituting the constituted transverse velocity, given by Eq. (51), into the continuity Eq. (45) and expanding the derivatives, we have

$$\frac{d\alpha_v}{d\tilde{y}} + \alpha_v \frac{\partial \ln \sqrt{\tilde{p}\tilde{\rho}}}{\partial \tilde{y}} + \frac{1}{\sqrt{\tilde{p}\tilde{\rho}}} \frac{\partial \tilde{\rho}}{\partial \tilde{x}} = 0. \tag{52}$$

The logarithmic term in general varies substantially slower than the linear terms and thereby can be neglected. Therefore, we have

$$\frac{d\alpha_v}{d\tilde{y}} + \frac{1}{\sqrt{\tilde{p}\tilde{\rho}}} \frac{\partial \tilde{\rho}}{\partial \tilde{x}} \approx 0. \tag{53}$$

Neglecting the correction due to the perturbation pressure, the partial derivatives $\partial \tilde{\rho}/\partial \tilde{x}$ and $\partial \tilde{T}/\partial \tilde{x}$ for uniform environment pressure are correlated through the equation of state for ideal gas, i.e.,

$$\frac{1}{\tilde{\rho}} \frac{\partial \tilde{\rho}}{\partial \tilde{x}} = -\frac{1}{\tilde{T}} \frac{\partial \tilde{T}}{\partial \tilde{x}}. \tag{54}$$

Substituting Eq. (54) into Eq. (53), we obtain an ordinary differential equation for α_v, i.e.,

$$\frac{d\alpha_v}{d\tilde{y}} \approx \frac{\tilde{B}}{\tilde{T}\sqrt{\tilde{p}/\tilde{\rho}}}(1 + \tilde{T}_e - \tilde{T}) \exp\left(-\frac{\tilde{T}_a}{\tilde{T}} \right), \tag{55}$$

where we have used the one-dimensional result for $\partial \tilde{T}/\partial \tilde{x}$ given by Eq. (14). Substituting Eq. (44) into Eq. (55) and using the principle of energy conservation for chemical reaction, i.e., $Qc_{F0} = \rho c_p \Delta T_{\text{reaction}}$, we can write

$$\frac{\tilde{p}}{\rho} = \frac{(\gamma - 1)c_p \Delta T_{\text{reaction}}}{U^2}(\tilde{T} - \tilde{T}_e) = \frac{1}{M_{\text{reaction}}^2}(\tilde{T} - \tilde{T}_e), \tag{56}$$

where the reaction Mach number $M_{\text{reaction}} = U/\sqrt{\gamma R \Delta T_{\text{reaction}}}$ represents the ratio of kinetic energy of the supersonic flow to the chemical heat release.

To solve Eq. (55), we need to know α_v at $\tilde{y} = 0$, which is specified as follows. The perturbation pressure initiates from the lower boundary with $\tilde{y} = 0$, where the chemical reaction proceeds with the highest rate due to the highest inlet temperature. In addition, as the reaction front advances in the transverse direction, it contributes to stronger perturbation pressure and thus larger transverse velocity. Therefore, we assume that the transverse velocity $\tilde{v}$ is an increasing function of transverse coordinate $\tilde{y}$ and $\tilde{v} = 0$ at $\tilde{y} = 0$. Consequently, the parameter α_v satisfies

$$\alpha_v = 0 \quad \text{at} \quad \tilde{y} = 0. \tag{57}$$

Integrating Eq. (55) with respect to y and using the boundary condition in Eq. (57), we obtain

$$\alpha_v = M_{\text{reaction}} \tilde{B} \int_0^{\tilde{y}} \frac{\exp(-\tilde{T}_a/\tilde{T})}{\tilde{T}} \left[\frac{1}{\sqrt{(\tilde{T} - \tilde{T}_e)}} - \sqrt{(\tilde{T} - \tilde{T}_e)} \right] d\tilde{y}'. \tag{58}$$

D. Revisiting reaction front in terms of α_v

The reaction front derived in two-dimensional formulation can be organized in a generalization in terms of the parameter α_v, which reduces identically to $\tilde{L}_{\text{reaction}}$ in the one-dimensional framework as $\alpha_v \to 0$. Substituting the constituted transverse velocity given by Eq. (51) into Eq. (50), we obtain

$$-\tilde{v} \frac{\partial T}{\partial \tilde{y}} = \frac{\alpha_v^2}{2} \tilde{B}(1 + \tilde{T}_e - \tilde{T}) \exp\left(-\frac{\tilde{T}_a}{\tilde{T}} \right). \tag{59}$$

Substituting Eq. (59) into Eq. (28), the reaction length in the revised two-dimensional flow, denoted by L'_{reaction}, shall be written in the form:

$$\tilde{L}'_{\text{reaction}} = \frac{1}{1 + \alpha_v^2/2} \int_{\tilde{T}_e}^{1+\tilde{T}_e} \frac{d\tilde{T}}{\tilde{B}(1 + \tilde{T}_e - \tilde{T}) \exp(-\tilde{T}_a/\tilde{T})} = \frac{\tilde{L}_{\text{reaction}}}{1 + \alpha_v^2/2}. \tag{60}$$

Equation (60) demonstrates that the reaction front in the revised two-dimensional flow shortens as the magnitude of the factor α_v increases. In the absence of transverse velocity v, i.e., $\alpha_v = 0$, the revised reaction length L'_{reaction} spontaneously reduces to that determined from one-dimensional analysis, given by Eq. (15).

The integral on the right-hand side of Eq. (58) cannot be solved analytically. Based on the characteristics of the transverse velocity, a practical estimation of α_v can be obtained. First, the direction of the transverse velocity depends on the sign of the temperature gradient at the inlet, i.e., $d\tilde{T}_e/d\tilde{y}$. For a negative transverse gradient with $d\tilde{T}_e/d\tilde{y} < 0$, the fluid element in the lower layer (smaller $\tilde{y}$ coordinate) is more reactive than that in the upper layer (larger $\tilde{y}$ coordinate). Therefore, the transverse velocity moves upward. For positive transverse gradient with $d\tilde{T}_e/d\tilde{y} > 0$, the expansion-induced transverse velocity is downward. Therefore, the transverse velocity $\tilde{v}$ moves in the opposite direction of the inlet temperature gradient, i.e., $\tilde{v} \sim -d\tilde{T}_e/d\tilde{y}$.

In the present situation, the transverse velocity is created by the perturbation pressure, which originates from the chemical heat release. This indicates that we may use the temperature growth for chemical reaction $\Delta \tilde{T}_{\text{reaction}}$ as the characteristic temperature to evaluate the integral on the right-hand side of Eq. (58). In addition, it is noted that the magnitude of the integral is dominated by the exponential term. Therefore, we neglect the contribution of terms involving the square root of temperature difference and approximate the factor α_v as

$$\alpha_v \approx -\tilde{y} \tilde{B} M_{\text{reaction}} \exp(-\tilde{T}_a) \frac{d\tilde{T}_e}{d\tilde{y}}. \tag{61}$$

Substituting Eq. (61) into Eq. (60), we obtain that

$$\tilde{L}'_{\text{reaction}} = \tilde{L}_{\text{reaction}} \left[1 + \frac{1}{2} \tilde{y}^2 M_{\text{reaction}}^2 \tilde{B}^2 \exp(-2\tilde{T}_a) \left(\frac{d\tilde{T}_e}{d\tilde{y}} \right)^2 \right]^{-1}. \tag{62}$$
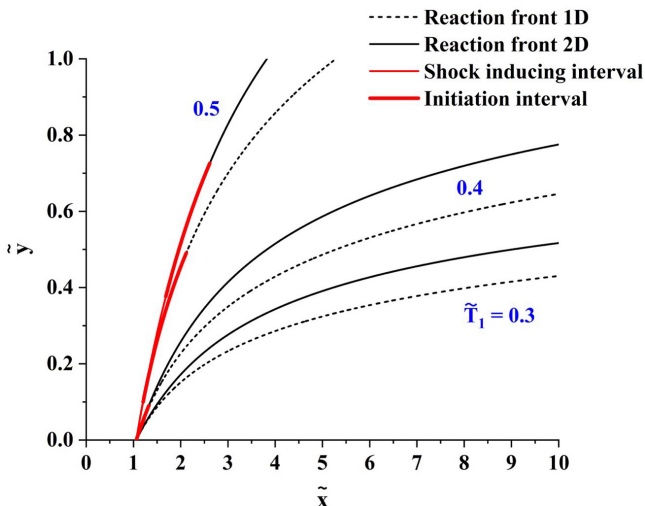
FIG. 11. Comparison of the reaction fronts determined based on one- and two-dimensional models. The reaction front and the induced shock wave are represented by the black solid line and the blue dashed line, respectively. The thickened red line refers to the initiation interval on the reaction front. The thermal nonuniformity is described by linear temperature distribution ($\alpha_T = 1.0$) at the inlet with fixed temperature at lower boundary $\tilde{T}_0 = 0.6$, and the temperatures at the upper bounds are $\tilde{T}_1 = 0.3$, $\tilde{T}_1 = 0.4$, and $\tilde{T}_1 = 0.5$.

The second term in the brackets represents the correction of reaction front due to the two-dimensional transverse flow. In the absence of thermal nonuniformity, i.e., $d\tilde{T}_e/d\tilde{y} \to 0$, the pressure perturbation becomes uniform in the whole field, which can hardly lead to two-dimensional transverse flow. Consequently, the magnitude of the parameter vanishes, i.e., $\alpha_v \to 0$, and the revised reaction front L'_{reaction} becomes identical to that obtained by one-dimensional formulation, i.e., $L'_{\text{reaction}} \to L_{\text{reaction}}$.

E. Detonation initiation in two-dimensional framework

Figure 11 compares the reaction fronts determined by one- and two-dimensional models, respectively. The reaction fronts predicted by the one-dimensional model are represented by dashed lines, while those revised by the two-dimensional framework are shown in solid lines. Both models start at the same point on the lower boundary of thermal nonuniformity, where the transverse velocity is assumed to vanish. In comparison with the one-dimensional results, the two-dimensional model introduces a more complex scenario by incorporating the effects of convective heat transfer in the transverse direction. As the reaction front moves forward, the heat generated by the exothermic reaction is not only conducted streamwise but also convected transversely.

The transverse heat transfer aids in distributing the thermal energy more effectively, which impacts the shape and progression of the reaction front. Specifically, the two-dimensional effect results in the concurrent shortening of the reaction length at each transverse coordinate. This implies that, for each position along the transverse axis, the distance over which the reaction occurs is reduced. This shortening effect is a direct consequence of the enhanced heat transfer in the transverse direction, which accelerates the reaction kinetics by maintaining higher temperatures across a broader region.

The initiation interval (thickened red line) and the shock-inducing interval (normal red line) are critical regions in the analysis. The shock-inducing interval refers to the regime on the reaction front that participates in shock wave generation. The initiation interval indicates the proportion of the reaction front that is sufficiently close to and thus forms the self-strengthening interaction with the
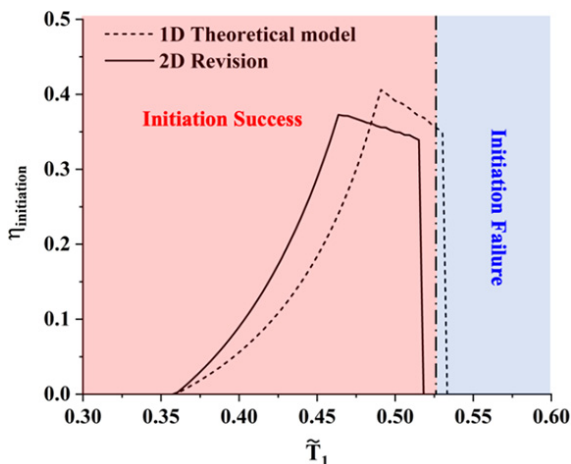
FIG. 12. The variation of detonation initiation factor with upper boundary temperature determined based on one- and two-dimensional models. The thermal nonuniformity is described by linear temperature distribution ($\alpha_T = 1.0$) at the inlet and the temperatures at the upper is fixed to be $\tilde{T}_0 = 0.60$.

induced shock wave, contributing to detonation initiation. The differences in these intervals between the one- and two-dimensional models highlight the importance of considering multidimensional effects in predicting the behavior of reaction fronts reasonably.

Figure 12 compares the variation of the detonation initiation factor with upper boundary temperature $\tilde{T}_1$. The distributions of $\eta_{\text{initiation}}$ with $\tilde{T}_1$ evaluated based on the one- and two-dimensional models almost share the same geometric profile. This indicates that the additional transverse convection hardly alters the underlying mechanism, leading to detonation initiation. Comparing with the one-dimensional results, $\eta_{\text{initiation}}$ determined by the two-dimensional formulation locates in a shorter regime of $\tilde{T}_1$. It can be understood that the transverse heat transfer promotes the thermal relaxation in that direction, which alleviates the streamwise bending of the reaction front. For strong thermal nonuniformity with large temperature difference, the shock-inducing interval is restricted to be a small portion of the reaction front close to the lower bound; thus, the alleviation of the reaction front bending due to the two-dimensional effect exhibits negligible influence on induced shock wave generation. Accordingly, the induced shock wave is of low intensity and thus inhibits the detonation initiation. For weak thermal nonuniformity with small temperature difference, the origin of the induced shock wave moves toward the upper bound, where the initiation interval can be found. Consequently, the alleviation of the reaction front bending may detach the induced shock wave from the reaction front. The interaction between the induced shock wave and the reaction front becomes weak, and as a result, the sudden fall of the reaction front occurs at smaller $\tilde{T}_1$. For intermediate thermal nonuniformity with appropriate temperature difference, both the induced shock wave and its interaction with the reaction front are optimized, resulting in the highest probability of detonation initiation, which is characterized by the peak value of the initiation factor. Regarding the numerical simulation results, the two-dimensional model yields a conservative prediction on the detonation initiation subject to thermal nonuniformity.

V. CONCLUDING REMARKS

In this paper, theoretical analysis is conducted for the detonation initiation induced by the thermal nonuniformity embedded at the inlet of a supersonic reactive flow. The underlying mechanism for detonation initiation is interpreted as follows. Passing through the thermal nonuniformity, the fluid elements entering the supersonic flow field at different transverse coordinates have different

temperatures, which causes the streamwise bending of the reaction front. The chemical heat release leads to the emission of pressure waves from the reaction front. Depending on the curvature of the reaction front, the pressure waves either collapse, forming an induced shock wave, or spread, propagating downstream. At suitable curvature, the induced shock wave locates in the vicinity of the reaction front, which facilitates chemical reaction and in turn enhances itself. The coherent coupling between chemical reaction and the induced shock wave consequently results in detonation initiation.

A detonation initiation factor $\eta_{\text{initiation}}$ is introduced to quantify the tendency of detonation initiation. It is defined as the proportion of the interval on the reaction front that contributes to induced shock wave formation and meanwhile participates in the self-strengthening interaction. The detonation initiation factor is in the range between 0 and 1. A higher value of $\eta_{\text{initiation}}$ corresponds to stronger capability of the thermal nonuniformity in causing detonation initiation. Depending on the intensity of thermal nonuniformity, quantified by $|\tilde{T}_0 - \tilde{T}_1|$, the detonation initiation changes drastically, which is revealed by the nonmonotonic variation of initiation factor. For fixed $\tilde{T}_0$, there exist three regimes, i.e., the initiation enhancing regime, the initiation saturation regime, and the initiation failure regime, in the phase space of $\eta_{\text{initiation}}$ and $\tilde{T}_1$. At the initiation enhancing regime, the streamwise bending of the reaction front alleviates as $\tilde{T}_1$ increases. It intensifies the induced shock wave and thereby leads to progressive growth of $\eta_{\text{initiation}}$. The initiation saturation regime is characterized by the slow variation of $\eta_{\text{initiation}}$ after reaching the maximum value. It can be attributed to the elevation of the induced shock wave toward the upper boundary so that the reaction fronts close to the lower boundary lose interaction with the induced shock wave. At sufficiently high $\tilde{T}_1$, the initiation failure regime is reached. The whole reaction front could be detached from the induced shock wave, and consequently, detonation can hardly be initiated.

It is found that the temperature profile of the thermal nonuniformity plays an important role in affecting detonation initiation. For upward convex temperature distribution, the curvature of the reaction front close to the lower boundary becomes alleviated. It considerably intensifies the induced shock wave and thus facilitates detonation initiation. The situation becomes complicated for downward convex temperature distribution. In this situation, the local curvature of the reaction front near $\tilde{y} = 0$ changes to be downward convex, while the rest remains upward convex. At low to moderate $\tilde{T}_1$, the severe bending of the reaction front near the lower boundary inhibits the formation of the induced shock wave, and consequently, detonation initiation cannot occur. At relatively high $\tilde{T}_1$, the downward convex portion of the reaction front produces an additional branch of an induced shock wave. It remains close to the reaction front over the whole transverse dimension of the thermal nonuniformity and thereby significantly extends the initiation interval. Accordingly, detonation initiation is substantially facilitated for relatively weak thermal nonuniformity with downward convex temperature distribution.

The pressure waves produced by chemical heat release are associated with transverse heat transfer, which affects the reaction front geometry and detonation initiation. In the two-dimensional formulation, the perturbation pressure field leading to convective transport in the transverse direction is obtained in analytical form. With knowledge of the perturbation pressure, the convective heat transfer in the transverse direction is evaluated. It is demonstrated that the transverse heat transfer lowers the curvature of the reaction front. The distribution of initiation factor $\eta_{\text{initiation}}$ predicted by the two-dimensional formulation slightly shrinks in the $\tilde{T}_1$ regime compared with that based on the one-dimensional analysis. The growth of $\eta_{\text{initiation}}$ at the initiation enhancing regime suggests that the convective heat transfer in the transverse direction tends to facilitate detonation initiation for relatively strong thermal nonuniformity with large temperature difference. The broadening of the initiation failure domain can be attributed to the weakening of the thermal nonuniformity due to the intensified thermal relaxation in the transverse direction.

This paper is based on the assumption of one-step global chemistry and uniform inlet flow with constant reactant concentration. In future studies, it would be interesting to consider the simplified thermal sensitive intermediate kinetics, e.g., Ref. [54], and to assess the impacts of reactant stratification on the detonation initiation process. Additionally, the spatial variation of flow velocity can noticeably change the geometry of the reaction front. It would also be interesting to

consider the nonuniformity of flow velocity and to underline its influence on detonation initiation in future works.

ACKNOWLEDGMENT

---

[1] F. A. Williams, *Combustion Theory* (CRC Press, Boca Raton, 2018).

[2] C. K. Law, *Combustion Physics* (Cambridge University Press, Cambridge, 2010).

[3] A. Liñán and F. A. Williams, *Fundamental Aspects of Combustion* (Oxford University Press, Oxford, 1993).

[4] P. Clavin and G. Searby, *Combustion Waves and Fronts in Flows: Flames, Shocks, Detonations, Ablation Fronts and Explosion of Stars* (Cambridge University Press, Cambridge, 2016).

[5] J. H. Lee, *The Detonation Phenomenon* (Cambridge University Press, Cambridge, 2008).

[6] P. Wolański, Detonative propulsion, Proc. Combust. Inst. **34**, 125 (2013).

[7] J. E. Shepherd, Detonation in gases, Proc. Combust. Inst. **32**, 83 (2009).

[8] K. Kailasanath, Recent developments in the research on pulse detonation engines, AIAA J. **41**, 145 (2003).

[9] W. H. Heiser and D. T. Pratt, Thermodynamic cycle analysis of pulse detonation engines, J. Propuls. Power **18**, 68 (2002).

[10] B. A. Rankin, M. L. Fotia, A. G. Naples, C. A. Stevens, J. L. Hoke, T. A. Kaemming, S. W. Theuerkauf, and F. R. Schauer, Overview of performance, application, and analysis of rotating detonation engine technologies, J. Propuls. Power **33**, 131 (2017).

[11] T.-H. Yi, J. Lou, C. Turangan, J.-Y. Choi, and P. Wolanski, Propulsive performance of a continuously rotating detonation engine, J. Propuls. Power **27**, 171 (2011).

[12] Z. Zhang, K. Ma, W. Zhang, X. Han, Y. Liu, and Z. Jiang, Numerical investigation of a Mach 9 oblique detonation engine with fuel pre-injection, Aerosp. Sci. Technol. **105**, 106054 (2020).

[13] J.-L. Cambier, H. Adelman, and G. P. Menees, Numerical simulations of an oblique detonation wave engine, J. Propuls. Power **6**, 315 (1990).

[14] R. Zhou and J.-P. Wang, Numerical investigation of flow particle paths and thermodynamic performance of continuously rotating detonation engines, Combust. Flame **159**, 3632 (2012).

[15] C. Segal, *The Scramjet Engine: Processes and Characteristics* (Cambridge University Press, Cambridge, 2009).

[16] Z. Zhang, C. Wen, C. Yuan, Y. Liu, G. Han, C. Wang, and Z. Jiang, An experimental study of formation of stabilized oblique detonation waves in a combustor, Combust. Flame **237**, 111868 (2022).

[17] P. Clavin and B. Denet, Analytical study of the direct initiation of gaseous detonations for small heat release, J. Fluid Mech **897**, A30 (2020).

[18] L. He and P. Clavin, On the direct initiation of gaseous detonations by an energy source, J. Fluid Mech **277**, 227 (1994).

[19] M. Liberman, M. Ivanov, A. Kiverin, M. Kuznetsov, A. Chukalovsky, and T. Rakhimova, Deflagration-to-detonation transition in highly reactive combustible mixtures, Acta Astronaut. **67**, 688 (2010).

[20] J. Lee and I. Moen, The mechanism of transition from deflagration to detonation in vapor cloud explosions, Prog. Energy Combust. Sci. **6**, 359 (1980).

[21] J. Lee, R. Knystautas, and N. Yoshikawa, Photochemical initiation of gaseous detonations, Acta Astronaut. **5**, 971 (1978).

[22] J. F. Clarke, D. R. Kassoy, and N. Riley, On the direct initiation of a plane detonation wave, Proc. R. Soc. Lond. A **408**, 129 (1986).

[23] G. Ciccarelli and S. Dorofeev, Flame acceleration and transition to detonation in ducts, Prog. Energy Combust. Sci. **34**, 499 (2008).

[24] Y. B. Zeldovich, Regime classification of an exothermic reaction with nonuniform initial conditions, Combust. Flame **39**, 211 (1980).

[25] C. Vázquez-Espí and A. Liñán, Fast, non-diffusive ignition of a gaseous reacting mixture subject to a point energy source, Combust. Theory Model **5**, 485 (2001).

[26] X. Gu, D. Emerson, and D. Bradley, Modes of reaction front propagation from hot spots, Combust. Flame **133**, 63 (2003).

[27] A. Sileem, D. Kassoy, and A. Hayashi, Thermally initiated detonation through deflagration to detonation transition, Proc. R. Soc. Lond. A **435**, 459 (1991).

[28] C. Chan, D. Lau, P. Thibault, and J. Penrose, Ignition and detonation initiation by shock focussing, AIP Conf. Proc. **208**, 161 (1990).

[29] G. Singh and J. F. Clarke, Transient phenomena in the initiation of a mechanically driven plane detonation, Proc. R. Soc. Lond. A **438**, 23 (1992).

[30] I. Glassman, R. A. Yetter, and N. G. Glumac, *Combustion* (Academic Press, Waltham, 2014).

[31] Y. N. Shebeko, S. Tsarichenko, A. Y. Korolchenko, A. Trunev, V. Y. Navzenya, S. Papkov, and A. Zaitzev, Burning velocities and flammability limits of gaseous mixtures at elevated temperatures and pressures, Combust. Flame **102**, 427 (1995).

[32] P. Dai, Z. Chen, S. Chen, and Y. Ju, Numerical experiments on reaction front propagation in n-heptane/air mixture with temperature gradient, Proc. Combust. Inst. **35**, 3045 (2015).

[33] Y. Fang, Z. Hu, H. Teng, Z. Jiang, and H. D. Ng, Numerical study of inflow equivalence ratio inhomogeneity on oblique detonation formation in hydrogen–air mixtures, Aerosp. Sci. Technol. **71**, 256 (2017).

[34] C. Qi, P. Dai, H. Yu, and Z. Chen, Different modes of reaction front propagation in n-heptane/air mixture with concentration non-uniformity, Proc. Combust. Inst. **36**, 3633 (2017).

[35] P. Dai, Z. Chen, and X. Gan, Autoignition and detonation development induced by a hot spot in fuel-lean and CO_2 diluted n-heptane/air mixtures, Combust. Flame **201**, 208 (2019).

[36] P. Dai, Z. Chen, X. Gan, and M. A. Liberman, Autoignition and detonation development from a hot spot inside a closed chamber: Effects of end wall reflection, Proc. Combust. Inst. **38**, 5905 (2021).

[37] J. Pan, S. Dong, H. Wei, T. Li, G. Shu, and L. Zhou, Temperature gradient induced detonation development inside and outside a hotspot for different fuels, Combust. Flame **205**, 269 (2019).

[38] M. B. Luong and H. G. Im, Prediction of the developing detonation regime in a NTC-fuel/air mixture with temperature inhomogeneities under engine conditions, Proc. Combust. Inst. **39**, 4979 (2022).

[39] P. Yang, H. D. Ng, H. Teng, and Z. Jiang, Initiation structure of oblique detonation waves behind conical shocks, Phys. Fluids **29**, 086104 (2017).

[40] L. Yang, L. Yue, Q. Zhang, and X. Zhang, Numerical study on the shock/combustion interaction of oblique detonation waves, Aerosp. Sci. Technol. **104**, 105938 (2020).

[41] H. Teng, C. Tian, Y. Zhang, L. Zhou, and H. D. Ng, Morphology of oblique detonation waves in a stoichiometric hydrogen–air mixture, J. Fluid Mech **913**, A1 (2021).

[42] C. Vazquez-Espi and A. Linan, Thermal-diffusive ignition and flame initiation by a local energy source, Combust. Theory Model **6**, 297 (2002).

[43] D. C. Alexander and J. P. Sislian, Computational study of the propulsive characteristics of a shcramjet engine, J. Propuls. Power **24**, 34 (2008).

[44] C. Huete, A. L. Sánchez, F. A. Williams, and J. Urzay, Diffusion-flame ignition by shock-wave impingement on a supersonic mixing layer, J. Fluid Mech **784**, 74 (2015).

[45] T. C. Lieuwen, *Unsteady Combustor Physics* (Cambridge University Press, Cambridge, 2012).

[46] M. P. Burke, M. Chaos, Y. Ju, F. L. Dryer, and S. J. Klippenstein, Comprehensive H_2/O_2 kinetic model for high-pressure combustion, Int. J. Chem. Kinet. **44**, 444 (2012).

[47] B. J. Mcbride, M. J. Zehe, and S. Gordon, NASA glenn coefficients for calculating thermodynamic properties of individual species, Report No. NASA/TP–2002-211556 (NASA Center for Aerospace Information, Hanover, 2002), https://ntrs.nasa.gov/citations/20020085330.

[48] A. P. Dowling and Y. Mahmoudi, Combustion noise, Proc. Combust. Inst. **35**, 65 (2015).

[49] M. J. Zucrow and J. D. Hoffman, *Gas Dynamics. Volume 2-Multidimensional Flow* (John Wiley and Sons, New York, 1977).

[50] J. Lee and A. Higgins, Comments on criteria for direct initiation of detonation, Philos. Trans. Royal Soc. A. **357**, 3503 (1999).

[51] A. Bartenev and B. Gelfand, Spontaneous initiation of detonations, Prog. Energy Combust. Sci. **26**, 29 (2000).

[52] H. W. Liepmann and A. Roshko, *Elements of Gasdynamics* (Dover, Mineola, 2001).

[53] P. Yang, D. Yu, Z. Chen, H. Teng, and H. D. Ng, Effects of thermal stratification on detonation development in hypersonic reactive flows, Phys. Rev. Fluid **9**, 083202 (2024).

[54] H. Zhang and Z. Chen, Spherical flame initiation and propagation with thermally sensitive intermediate kinetics, Combust. Flame **158**, 1520 (2011).